

# Engineered 2D Transition Metal Dichalcogenides—A Vision of Viable Hydrogen Evolution Reaction Catalysis

Liangxu Lin,\* Peter Sherrell, Yuqing Liu, Wen Lei, Shaowei Zhang, Haijun Zhang, Gordon G. Wallace, and Jun Chen\*

The hydrogen evolution reaction (HER) is an emerging key technology to provide clean, renewable energy. Current state-of-the-art catalysts still rely on expensive and rare noble metals, however, the relatively cheap and abundant transition metal dichalcogenides (TMDs) have emerged as exceptionally promising alternatives. Early studies in developing TMD-based catalysts laid the groundwork in understanding the fundamental catalytically active sites of different TMD phases, enabling a toolbox of physical, chemical, and electronic engineering strategies to improve the HER catalytic activity of TMDs. This report focuses on recent progress in improving the catalytic properties of TMDs toward highly efficient production of H<sub>2</sub>. Combining theoretical and experimental considerations, a summary of the progress to date is provided and a pathway forward for viable hydrogen evolution from TMD driven catalysis is concluded.

of any known fuel (gravimetric energy density of 120–142 MJ kg<sup>-1</sup>).<sup>[2,3]</sup> Currently, the global H<sub>2</sub> production required to meet the industry need is around 0.1 gigatons, which is mainly consumed in ammonia production (54%), chemical production (35%), electronics processing (6%), metals processing/refining (3%), and food industry (2%).<sup>[4]</sup> The global need for H<sub>2</sub> as a fuel will continue to grow, as implementation into broader society via domestic consumption (e.g., power generation and heating) and transport industry (e.g., fuel driving vehicle) is accelerated. This growing need requires developments in H<sub>2</sub> storage, transport, and production techniques. While great progress has been made in H<sub>2</sub> storage and transport, the utilization of the H<sub>2</sub> energy is stymied by the lack of inexpensive and efficient production methods.

Current technologies producing H<sub>2</sub> are hydrocarbon reforming, pyrolysis of fossil fuels (e.g., natural gas, oil, and coal), and biomass conversion, which are expensive and unsustainable with significant greenhouse emissions.<sup>[2,3]</sup> An attractive alternative technique is water splitting which produces only H<sub>2(g)</sub> and O<sub>2(g)</sub> via direct thermolysis (>2500 °C), photocatalytic, or electrolytic routes. All of these water splitting techniques involve suitable catalysts to improve the production of H<sub>2</sub> and reduce the energy consumption, yet electrolysis is the most encouraging technique owing to its high efficiency and relatively low cost.<sup>[2–4]</sup> The half reaction of water splitting to produce H<sub>2(g)</sub> via electrolysis is called the electrochemical hydrogen evolution reaction (HER).

It is believed that the electrochemical HER will be key to meeting global challenges of the energy crisis and anthropogenic climate change, giving uninterrupted H<sub>2(g)</sub> fuel supplies with low energy consumption.<sup>[5,6]</sup> Currently, the most efficient HER catalysts are precious metal (e.g., Pt and Pd) based which are expensive and scarce. Recently, a new class of catalytic materials, layered transition metal dichalcogenides (TMDs), have emerged with several advantages over noble metal catalysts, notably the lower cost and higher abundance. Results showed that these sustainable materials are promising catalysts for the HER.<sup>[7,8]</sup> Early studies on developing these catalytic materials were stymied by the low efficiency due to the scarcity of metal edge sites and the poor electron transport efficiency in multi-layered TMDs.<sup>[9,10]</sup> In recent years, research progress in using TMDs as HER catalysts has developed rapidly, led by improved

## 1. Introduction

Tackling global climate change and the energy crisis requires novel approaches in clean energy generation and efficient manufacturing.<sup>[1]</sup> Hydrogen (H<sub>2</sub>) is one of the most popular clean energy sources, providing the highest energy output

Dr. L. Lin, Dr. W. Lei, Prof. H. Zhang  
The State Key Laboratory of Refractories and Metallurgy, and Institute of Advanced Materials and Nanotechnology  
Wuhan University of Science and Technology  
Wuhan 430081, China  
E-mail: liangxu@uow.edu.au

Dr. L. Lin, Dr. Y. Liu, Prof. G. G. Wallace, Prof. J. Chen  
ARC Centre of Excellence for Electromaterials Science  
Intelligent Polymer Research Institute  
Australia Institute for Innovative Materials (AIIM)  
Innovation Campus  
University of Wollongong  
Squires Way, North Wollongong, NSW 2519, Australia  
E-mail: junc@uow.edu.au

Dr. P. Sherrell  
Department of Chemical Engineering  
The University of Melbourne  
Parkville, VIC 3000, Australia

Prof. S. Zhang  
College of Engineering  
Mathematics and Physical Sciences  
University of Exeter  
Exeter EX4 4QF, UK

 The ORCID identification number(s) for the author(s) of this article can be found under <https://doi.org/10.1002/aenm.201903870>.

DOI: 10.1002/aenm.201903870

fundamental understandings in the catalytic process and advancements in chemical, electronic, and structural tuning of TMDs. In this progress report, we provide a background to key concepts for the electrochemical HER and discuss how TMDs can be manipulated through size, strain, defect, and phase engineering; edge-enrichment strategies; chemical doping; and hybrid structures to unlock their potential as the next-generation of HER catalysts.

## 2. Key Concepts of Electrochemical HER

### 2.1. HER at Electrodes

Complete water splitting can be described by the overall reaction (1)



where the full reaction includes two half-reactions, the reduction reaction to generate  $\text{H}_2$  (HER) at the cathode electrode and the oxidation reaction to generate  $\text{O}_2$  (oxygen evolution reaction/OER) at the anode electrode. Conventionally research is driven in the acidic regime (anode:  $\text{H}_2\text{O} \rightarrow 2\text{H}^+ + \frac{1}{2}\text{O}_2 + 2\text{e}^-$ ; cathode:  $2\text{H}^+ + 2\text{e}^- \rightarrow \text{H}_2$ ), and the HER in this case normally involves three steps:

- i) the Volmer reaction on the electrode surface, giving the reaction between a proton and the transferred electron to generate an adsorbed hydrogen atom ( $\text{H}_{\text{ads}}^*$ );
- ii) the Tafel reaction which combines two adsorbed H atoms to generate  $\text{H}_2$  gas, or
- iii) the Heyrovsky reaction involving the reaction between one adsorbed H atom, one electron and one proton to yield  $\text{H}_2$  gas.

The Volmer reaction is the first reaction to generate the necessary adsorbed intermediate, and is typically rate-limiting step of HER. In principle, electrochemical water splitting (or HER) requires a thermodynamic electrochemical potential of  $\approx 1.23$  V at room temperature. This value increases under experimental conditions when the high activation energy ( $E_a$ ) is required to form reaction intermediates on the electrode surface. This is where the catalyst provides value by minimizing the overpotentials (energy cost) at the electrodes for both HER and OER by reducing the thermodynamic barriers, and thus accelerates the overall reaction.

### 2.2. Key Principles for the HER (in Acidic Media)

In electrochemical HERs, the catalytic performance of a catalyst is normally measured by the HER current density ( $j$ ) at certain overpotentials. A good HER catalyst should exhibit high  $j$  at low overpotentials. This HER performance is a synergic result of both the catalytic activity and the number of the active sites.<sup>[10]</sup> In practical cases, the reaction kinetics (e.g., the activation energy,  $E_a$ ) and mass transfer are also affect the HER process



**Liangxu Lin** is currently a vice-chancellor fellow at the University of Wollongong. He completed his Ph.D. in Engineering Materials at The University of Sheffield at the end of 2013. After two postdoc periods at the University of Exeter, he joined Wuhan University of Science and Technology as a professor. His research focuses

on 2D nanomaterials for electrochemical energy storage/conversion, catalysis, and materials interfaces.



**Jun Chen** is currently a full professor at IPRI|ACES, Australian Institute for Innovative Materials, University of Wollongong (UOW). He received B.E. from Zhejiang University of Technology (1995) and Ph.D. from UOW (2003), and published more than 190 papers. His research interests include sustainable energy devices,

electro-/bio-interfaces, nano/micromaterials, 2D/3D printing, and smart wearable electronic devices.

greatly. As we have introduced above, the Volmer and Heyrovsky reactions all perform the proton–electron transfer process which are highly dependent on the electrode potential. The electrode potential changes with the electrostatic potential of the water–solid interface, and highly depends on different hydrogen atoms added on the electrode.<sup>[11–13]</sup> Triggering the Volmer, Tafel, or Heyrovsky reactions requires overcoming the particular energy barrier for that specific reaction at the electrode, and the  $E_a$  can be extrapolated to the limit where the potential does not change.<sup>[12,14,15]</sup> Building on this principle, Tang and Jiang calculated the reaction energy ( $\Delta E$  between the final and initial states), the  $E_a$  of the above three elementary steps of 1T MoS<sub>2</sub>, and suggested that the full HER is rate limited by the desorption of the H since the  $E_a$  of the Heyrovsky reaction ( $E_a = 0.62$  eV) is much higher than that of the Volmer step ( $E_a = 0.16$  eV), and lower than that of the Tafel reaction ( $E_a > 0.89$  eV).<sup>[12]</sup>

Nevertheless, the Volmer reaction is the rate limiting step in most HERs, and the Sabatier principle provides good guidance in designing suitable materials with the consideration of the free-energy of adsorbed H on the active site ( $\Delta G_{\text{H}^*}$ ) during an equilibrated reaction.<sup>[7]</sup> With this principle, a good HER catalyst should satisfy the criterion of suitable  $\Delta G_{\text{H}^*}$  which is closest to that of the reactant or product ( $\Delta G_{\text{H}^*} \approx 0$ ). The reaction is rate limited by the adsorption of  $\text{H}^*$  if  $\Delta G_{\text{H}^*}$  is too high (insufficient binding), and in turn is  $\text{H}_2$ -desorption limited provided a too negative  $\Delta G_{\text{H}^*}$  (binding is too strong).

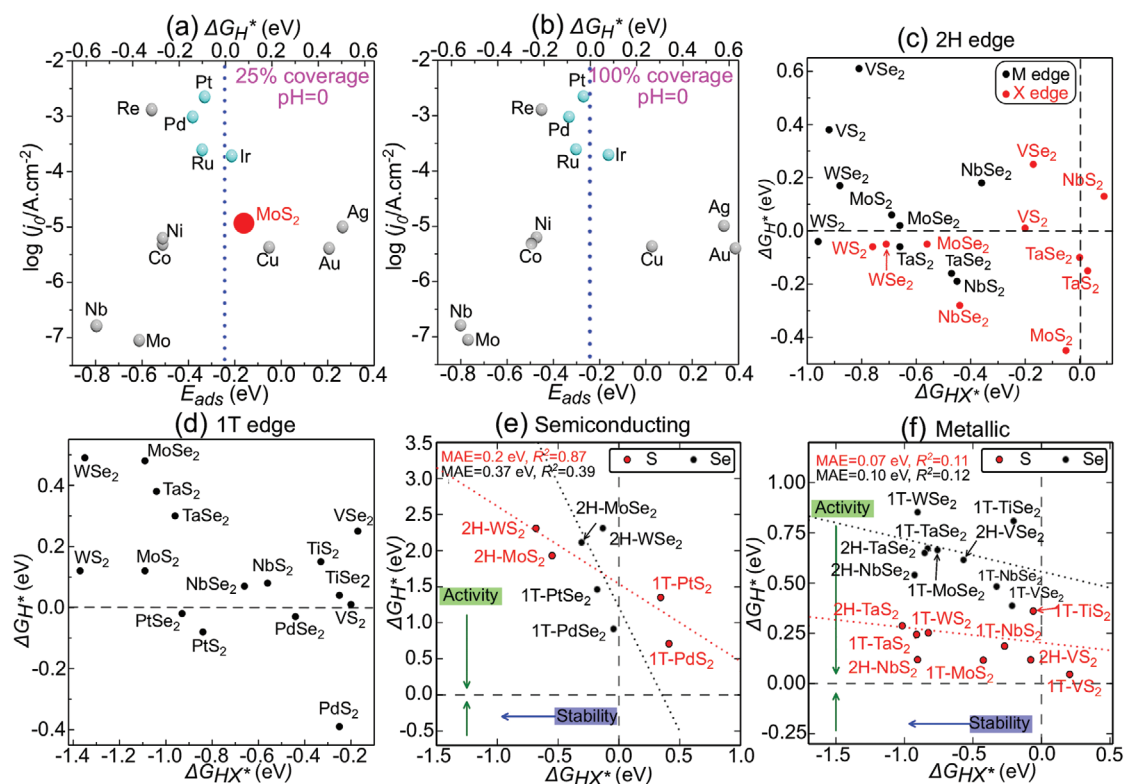


**Figure 1.** The Sabatier plot shows the  $j_0$  against the  $\Delta G_{H^*}$  and  $E_{ads}$  of different metals with a) 25% and b) 100% H coverages at pH = 0. Data was taken from refs. [8,19]. Materials near the top and close to the  $\Delta G_{H^*}$  of 0 eV are expected to be most active in HER. The  $j_0$  of many reported MoS<sub>2</sub> materials is also highlighted in (a), which is similar to some other TMDs.<sup>[8,19]</sup> Plots of the  $\Delta G_{H^*}$  as a function of the HX adsorption free energy ( $\Delta G_{HX^*}$ , X = S or Se) at c) 2H edge, d) 1T edge, e) 2H plane, and f) 1T plane. Data in (c,d) is taken from refs. [22–24]. MAE is the mean absolute error. The dotted lines are guides for the eye. (e,f) are reproduced with permission.<sup>[24]</sup> Copyright 2015, Elsevier.

In most literature, the HER catalytic activity of a material is usually described by the parameters of Tafel slope,  $j_0$ , turnover frequency (TOF) and onset overpotential. The former two represent the relationship between the overpotential ( $\eta$ ), current density ( $j$ ) and  $j_0$  as the following equation<sup>[16]</sup>

$$|\eta| = \frac{2.3RT}{\alpha nF} \log \frac{j}{j_0} \quad (2)$$

where  $R$ ,  $T$ ,  $\alpha$ ,  $n$ , and  $F$  are the ideal gas constant, the absolute temperature, the electrochemical transfer coefficient, the number of electrons involved in the reaction and the Faraday constant, respectively. The Tafel slope is defined as the value of  $\frac{2.3RT}{\alpha nF}$  (mV dec<sup>-1</sup>).<sup>[16]</sup> The HER can be rate-limited by the Volmer, Heyrovsky, or Tafel reactions when the Tafel slope is about 120, 40, and 30 mV dec<sup>-1</sup>, respectively.<sup>[17]</sup>  $j_0$  is the value of the current density from the Tafel plot at the overpotential of 0 V, reflecting the intrinsic catalytic activity of the catalyst under equilibrium conditions.<sup>[16]</sup> The TOF is the value describing how many molecules are generated per active site per second (s<sup>-1</sup>), which is frequently used in the research of catalysis. In the HER, this value highly depends on the working potential. Since the polarization curve of the HER is the synergic result of different active sites, the TOF is an average of catalytic activity of all active sites. As for the onset overpotential, it

is the overpotential of the HER activity begins, and can be extrapolated from Tafel plot and the cathodic Tafel line.<sup>[10,18]</sup> However, many reports in literature use the overpotential as the onset overpotential where a defined current density (e.g., 10 mA cm<sup>-2</sup>) is reached, which is unsuitable as this value changes with the catalyst loading as well as the active site coverage. In this case, the term of catalytic performance might be used to distinguish with the catalytic activity, and more direct, suitable methods (e.g., Faradaic and energy efficiencies) should be introduced to estimate the total catalytic performance.

Building on these key principles, the best HER catalyst developed so far are still noble metal based. For example, except the high exchange current density ( $j_0$ ), also represents the kinetics toward the redox reaction of the catalyst,<sup>[16]</sup> Pt has  $\Delta G_{H^*}$  around -0.09 and -0.03 eV at pH = 0 with a 25% and 100% H coverage, respectively (Figure 1a,b).<sup>[19]</sup> Nevertheless, with an abundance of chemistries, electronic structures, and properties, the cheap and abundant TMDs, have emerged as leading materials for the next generation of HER catalysis.<sup>[7–10,20–24]</sup> TMDs can have a  $\Delta G_{H^*}$  close to 0 eV, a high  $j_0$  (Figure 1c–f, will be further introduced), and a fundamental competitive advantage over competing emerging HER catalysts in that they have rich tunable 2D surface chemistries, and more importantly, precisely tunable properties based on size, defects, strain, doping, and heterostructure formation on the 2D planar crystals. The

progress in tailoring TMDs via these strategies forms the basis for our discussions within the progress report. Building on the progress we have achieved so far, comparison of the TMDs with other state-of-the-art HER catalysts, and the future possibilities on developing highly efficient TMD based HER catalysts are also included in this report.

### 3. TMD Materials as Catalysts for the HER

TMDs are materials having chemical composition of  $\text{MX}_2$  (M and X are the transition metal and the chalcogen, respectively, including similar chalcogenides with more than one TM atom and corresponding X atoms) with 2D building blocks (e.g., S–Mo–S) weakly bonded to each other by van der Waals forces (Figure 2). There are three crystal phases that most TMD monolayers are thermodynamically stable (Figure 2a,b); 1H for most group VI TMDs ( $D_{3h}$  point group, each M center is prismatically coordinated by six surrounding X atoms); 1T phase for group IV, VII, and X TMDs ( $D_{3d}$  group, M atom is octahedrally coordinated to six neighboring X atoms); and 1T' (or  $T_d$ ) for  $\text{WTe}_2$  where the 1T lattice is distorted.<sup>[21–24]</sup> However, TMDs can be switched between phases and “locked” into a metastable phase, for example  $\text{MoS}_2$  into 1T via lithium exfoliation and charge injection<sup>[25]</sup> or  $\text{WSe}_2$  into 1T' by controlled cooling rates and ligand selection.<sup>[26]</sup> The earliest reports of TMDs for electrochemical water-splitting come from the late 1970s.<sup>[27]</sup> The explosion of interest in TMD materials corresponds to the development of exfoliation<sup>[28]</sup> and synthesis<sup>[29,30]</sup> techniques that have enabled the production and stabilization of monolayers. These monolayers enable a higher per mass catalytically active surface area, and thus more catalytically active basal-plane, defect, and edge sites available for the HER to occur.

Bulk TMDs can be stacked from the monolayers and commonly have three polymorphs (1T, 2H, and 3R/rhombohedral), depending on the crystal phase and stacking arrangement. The number in these three polymorphs means how many M–X–M units in the unit cell of the bulk crystal. The physical properties of the bulk TMDs are varied.<sup>[22–24]</sup> For example, group 5 TMDs could be either 1T or 2H structured. For group 4, 7, and 10 bulk TMDs in the periodic table (Figure 2a), it prefer the 1T phase, whereas the group 6 TMDs prefer the 2H phase.<sup>[22–24]</sup> Some TMDs such as groups 4 and 5 are metallic, and some are semiconducting (groups 6, 7, and 10).<sup>[22–24]</sup>

The HER catalytic activity and mechanism of metallic and semiconducting sites of TMDs are significantly different from each other. Although the basal plane of 1H/2H-TMDs such as  $\text{MoS}_2$ ,  $\text{WS}_2$ ,  $\text{MoSe}_2$ , and  $\text{WSe}_2$  are HER inert ( $\Delta G_{\text{H}^*}$  is  $\approx 2$  eV uphill),<sup>[22]</sup> the  $\Delta G_{\text{H}^*}$  at the metallic edge (the edge performers metallic features) in some cases is close to that of Pt and is thermo-neutral (Figure 1c).<sup>[7]</sup> It was revealed that the  $\Delta G_{\text{H}^*}$  of 2H- $\text{MoS}_2$ 's edge is close to 0.08 eV with 50% H coverage (the  $j_0$  of some reported 2H  $\text{MoS}_2$  is also high).<sup>[7]</sup> The result has been further refined, giving the best edge configurations of  $\text{MoS}_2$  (0.06 eV of  $\Delta G_{\text{H}^*}$ ) and  $\text{WS}_2$  (–0.04 eV of  $\Delta G_{\text{H}^*}$ ) with 50% S coverage, versus  $\Delta G_{\text{H}^*}$  of –0.45 and –0.06 eV respectively in both cases with 100% S edges.<sup>[22]</sup>

Figure 1c,d are the plot of  $\Delta G_{\text{H}^*}$  of various TMDs at different edges against the absorption free energy of H-X ( $\Delta G_{\text{HX}^*}$ ; X is the chalcogen) based on the data reported by Tsai et al.<sup>[22–24]</sup> The reaction tends to form  $\text{H}_2\text{X}$  along with the desorption of H-X group when  $\Delta G_{\text{HX}^*} > 0$ ; whereas it would be more stable upon decreasing the  $\Delta G_{\text{HX}^*}$ . Besides  $\text{MoS}_2$ , several other TMDs such as  $\text{MoSe}_2$ ,  $\text{WS}_2$ ,  $\text{WSe}_2$ , and  $\text{TaS}_2$  are also highly promising for HER with 2H or 1T edges (Figure 1c,d). Tsai et al. have further calculated the  $\Delta G_{\text{H}^*}$  and  $\Delta G_{\text{HX}^*}$  at both the edge and basal plane of various TMDs to estimate the HER catalytic activity and relating stability.<sup>[22,23]</sup>  $\Delta G_{\text{H}^*}$  at the edge of TMDs are all close to 0 eV and highly suited for HER, while the  $\Delta G_{\text{HX}^*}$  of all 1T and most 1H/2H edges are negative (Figure 1c,d).<sup>[24]</sup> The  $\Delta G_{\text{H}^*}$  on the basal plane of semiconducting TMDs is normally high and unsuitable for HER (e.g.,  $\Delta G_{\text{H}^*}$  of  $\approx 1.92$  eV of the 2H  $\text{MoS}_2$ ).<sup>[24]</sup> Replacing the Se by S (electronegativity: 2.58 of S vs 2.55 of Se) in TMDs can slightly tune the  $\Delta G_{\text{H}^*}$  close to more thermo-neutral states, but which on the other hand reduces the stability significantly (Figure 1e). The stability of the semiconducting basal plane should be carefully considered during the activation for an efficient HER. Like that on the semiconducting basal plane, the  $\Delta G_{\text{H}^*}$  on the metallic plane has also the inverse relationship with  $\Delta G_{\text{HX}^*}$  (Figure 1f).<sup>[24]</sup> Nevertheless, the metallic planes are more active for the HER with similar stabilities comparing with the semiconducting basal plane, i.e., the  $\Delta G_{\text{H}^*}$  of 0.12 eV on the plane of 1T- $\text{MoS}_2$  versus the 1.92 eV on that of the 1H/2H- $\text{MoS}_2$ .<sup>[24]</sup> In this case, improving the electronegativity of the X atoms (e.g., replacing the Se by S) can be more efficient to improve the HER activity than that on the semiconducting TMDs (at the basal plane), and the basal plane of some metallic TMDs are actually suited for catalytic HER (Figure 1f), i.e., both the 1T- $\text{MoS}_2$  and 2H- $\text{NbS}_2$  have the  $\Delta G_{\text{H}^*}$  of around 0.12 eV on the basal plane, which is close to the 2H edges of some TMDs (e.g.,  $\text{MoS}_2$ , Figure 1c). Some TM sulfides are not chemically stable in aqueous media ( $\Delta G_{\text{HX}^*}$  of 0.21 and –0.09 eV on the basal plane of 1T- $\text{VS}_2$  and 1T- $\text{TiS}_2$ , respectively, Figure 1f), however if they can be stabilized the  $\Delta G_{\text{H}^*}$  values are highly promising for efficient HER (e.g., 0.05 eV of 1T- $\text{VS}_2$  and 0.38 eV of 1T- $\text{TiS}_2$ ).<sup>[24]</sup> These features open new avenues to robust and stable HER, if the  $\Delta G_{\text{H}^*}$  and  $\Delta G_{\text{HX}^*}$  can be further adjusted (e.g., by the chemical doping) toward more stable surfaces with a  $\Delta G_{\text{H}^*}$  more close to 0.

Despite these theoretical calculations, research on the experimental HER performance of TMDs is rather limited before 2010 because of the very poor catalytic activity. Such poor performance was mainly due to at least the following two reasons:

- the scarcity of edge sites, which are the only catalytically active part of the material in most cases and
- the low electrical conductivity of the most TMDs.<sup>[6,9]</sup> For example, the HER catalytic activity of 2H  $\text{MoS}_2$  decreases by a factor of  $\approx 4.5$  with each additional layer due to the poor electron hopping efficiency in multilayers (Figure 2c).<sup>[9]</sup> The understanding of these limitations, in combinations with the ability to tune the electronic and chemical properties of TMDs, provides a clear direction to improve and use TMDs as HER catalysts. It is from these tuning methods that tailored strategies to improve the HER catalytic activity can be developed (Figure 2d).

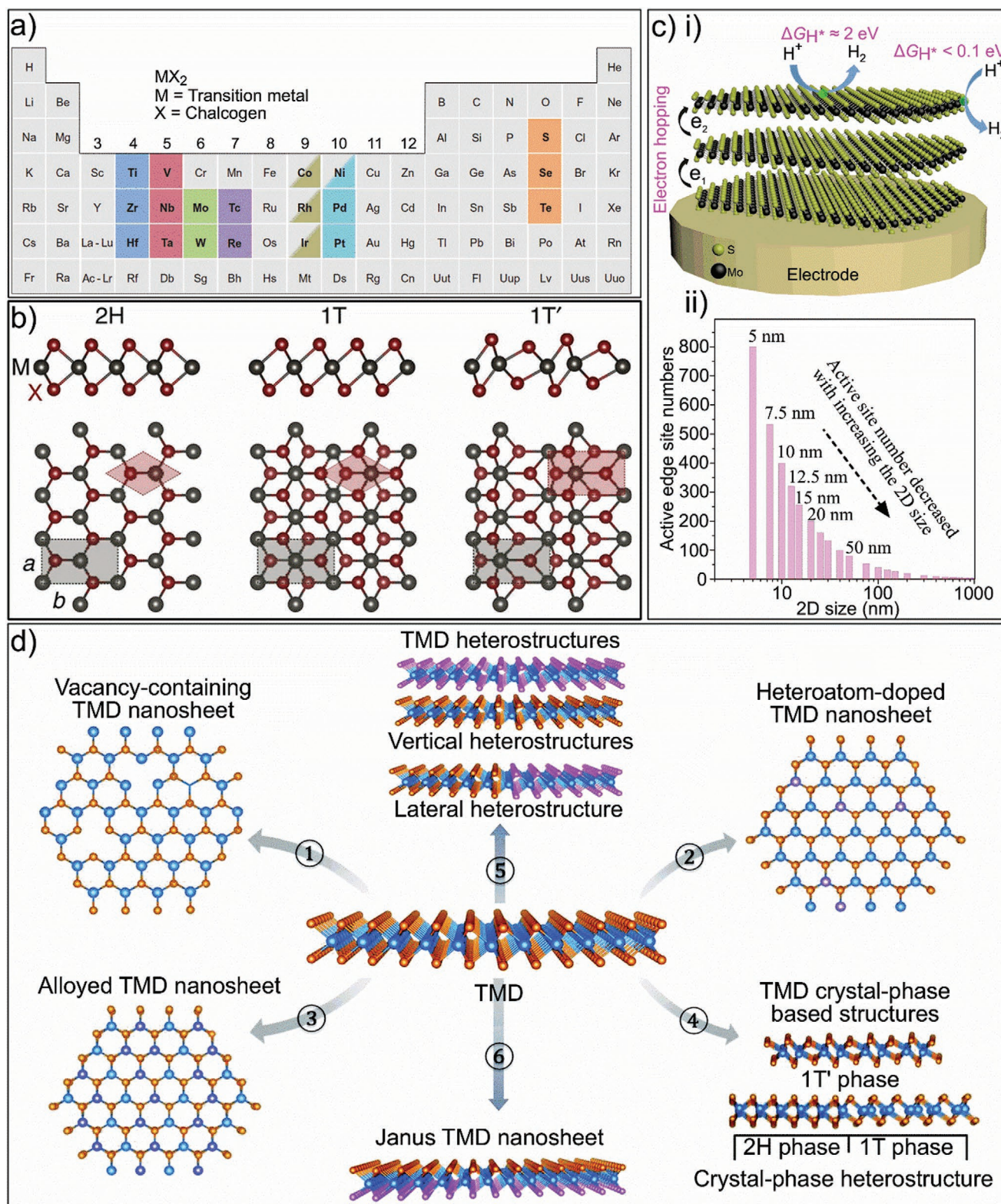


**Figure 2.** a) The periodic table with TMD elements highlighted. Reproduced with permission.<sup>[21]</sup> Copyright 2013, Springer Nature. b) The three most common crystal structures for TMDs, 2H, hexagonal, 1T, octahedral, and 1T', distorted octahedral, each with different electronic properties. Reproduced with permission.<sup>[31]</sup> Copyright 2016, Springer Nature. c) i) Electron hopping in multilayered 2H-MoS<sub>2</sub> and the  $\Delta G_{H^+}$  at basal plane and edge sites. ii) the number of catalytically active sites as a function of size for equal amount of material. d) Methods to tune the chemistry, electronic, and catalytic properties of TMD monolayers by defect engineering, bandgap engineering, and heterostructure formation. Reproduced with permission.<sup>[32]</sup> Copyright 2018, Royal Society of Chemistry.

## 4. Progress on Strategies to Improve the HER Catalytic Activity of 2D TMDs

The fundamental understanding gained over the past few years in the catalytically active sites, reaction limiting factors, and the importance of precise chemical and structural control of TMDs has opened a clear set of opportunities to manipulate their properties toward increased catalytic activity. These include precise phase control, defect generation, size control and edge enrichment, chemical doping, heterostructuring, and any combination of these (Figure 2d). Before the discussion of this progress, we briefly revisit the development on multilayered TMDs as the HER catalyst over the last decade. Improvements on the catalytic performance have been realized via the following strategies:

- i) the formation of nanomaterials and amorphous phases;<sup>[33–41]</sup>
- ii) the edge-aligned TMDs,<sup>[42–51]</sup> and
- iii) 3D porous TMDs.<sup>[52–59]</sup>

Although the formation of the TMDs nanoparticle can directly improve the edge ratio, the catalytic performance is still quite poor due to the poor electron hopping between the multilayers (Figure 2c).<sup>[33–37]</sup> The poor charge transport might be alleviated in amorphous TMDs, while the density of the active site also increased dramatically. Some amorphous TMDs have exhibited outstanding catalytic performance,<sup>[38–41]</sup> comparable to lately developed 2D TMDs. Nevertheless, their poor stability/durability associated with the amorphous nature is still needed to be addressed suitably. Besides, both the edge aligned and 3D TMDs have been introduced in terms to improve the catalytic performance. These approaches have been further modified by expanding the layer distance and introducing strain into the lattice,<sup>[51,54]</sup> but the performance is still unsatisfactory. Technical challenges limiting these approaches are the inert plane on the 3D channel, and the poor charge transport issue between the edge aligned multilayered TMDs.

Unlike these multilayered TMDs, the 2D TMDs (e.g., monolayers) are more active owing to the increased charge transport efficiency (Figure 2c), the higher exposed surface areas, and the rich surface chemistry, which enables various strategies (discussed below) to improve the catalytic performance.

### 4.1. Phase Engineering

As we mentioned above, TMDs are unique layered materials. The 2D monolayered building blocks of TMDs exist in one of three phases (1H, 1T, and 1T', Figure 2b). All of these 2D TMDs have dramatically different electronic properties and catalytic activity. The thermodynamically stable form of MoS<sub>2</sub>, WS<sub>2</sub>, MoSe<sub>2</sub>, and WSe<sub>2</sub> is 1H (or 2H), and for all of these materials 1H (or 2H) is semiconducting and hence has quite poor electrical conductivity. Manipulation of these materials can lead to the formation of the 1T metallic TMDs which has different catalytically active sites and significantly improved electron transport efficiency. Further, theoretical calculations have suggested that the basal plane of some 1T TMDs (e.g., MoS<sub>2</sub>, NbS<sub>2</sub>, VS<sub>2</sub>, TaS<sub>2</sub>, WS<sub>2</sub>, TiS<sub>2</sub>) are catalytically active for HER, whereas the basal plane of their 1H/2H phases are usually inert due to

the high  $\Delta G_{H^*}$  (Figure 1c–f).<sup>[22–24]</sup> The key challenges to explore for 1T TMDs monolayers are the stability and cheap methods of production.

In 2013, Chhowalla and co-workers reported the HER of chemical exfoliated WS<sub>2</sub> monolayers with both 1T and 1H structures (Figure 3).<sup>[60]</sup> Testing thin films of 1H WS<sub>2</sub> showed with onset overpotentials of 150–200 mV and a Tafel slope of 110 mV dec<sup>-1</sup> or higher. Increasing the 1T WS<sub>2</sub> concentration (1H WS<sub>2</sub> ratio decreased) gradually improved the HER performance (Figure 3a–d).<sup>[60]</sup> Among different WS<sub>2</sub> samples, 1T WS<sub>2</sub> monolayers exhibited the best HER performance, giving the Tafel slope of 55 mV dec<sup>-1</sup> (was 60 mV dec<sup>-1</sup> without *iR* correction), onset overpotential of 80–100 mV and a  $j_0$  of  $2 \times 10^{-5}$  A cm<sup>-2</sup>.<sup>[60]</sup>

This HER performance of WS<sub>2</sub> monolayers (particularly the 1H monolayers) might be underestimated since the catalyst was mounted on the glassy carbon electrode with the thickness larger than five monolayers.<sup>[60]</sup> For 1H semiconducting monolayers, the thickness of the catalyst on the electrode should be ideally as thin as the monolayer to sustain the rapid charge transport between the electrode and the top-most surface of the catalyst. Re-stacking of the monolayers would degenerate the HER performance.<sup>[10]</sup> Therefore, the relationship between the catalytic performance and the loading amount of monolayered Mo-S nanocrystals (NCs) on the glassy carbon electrode is crucial.<sup>[10]</sup> The double layer capacitance ( $C_{dl}$ ) (reflects the effective surface area of the total active sites) divided by the catalyst mass gradually decreased by increasing the catalyst loading.<sup>[10]</sup> With a mass density larger than  $\approx 100$   $\mu\text{g cm}^{-2}$ , the  $C_{dl}$  was decreased by adding more catalyst. All these features meant that the re-stacking/agglomeration of monolayered NCs highly suppressed the catalytic performance, i.e., the Tafel slope was also increased.<sup>[10]</sup>

The HER performance of 1H WS<sub>2</sub> monolayers with different sizes (edge lengths of 400–800 nm) has also been explored.<sup>[61]</sup> The monolayers were fabricated on Au foil by a chemical vapor deposition (CVD) method, and were directly used for the HER. Tafel slopes and  $j_0$  of these monolayers were 102–104 mV dec<sup>-1</sup> and 6.31–17.78  $\mu\text{A cm}^{-2}$ , respectively. Such exchange current density ( $j_0$ ) is comparable to that of 1T WS<sub>2</sub> nanosheets ( $2 \times 10^{-5}$  A cm<sup>-2</sup>),<sup>[60]</sup> owing to the interaction between the Au foil and WS<sub>2</sub>.<sup>[61]</sup> In comparison, 1H MoS<sub>2</sub> monolayers grown on Au foils has the Tafel slope of 61 mV dec<sup>-1</sup> and the  $j_0$  of 38.1  $\mu\text{A cm}^{-2}$ , a significant improvement compared to WS<sub>2</sub> with smaller size.<sup>[62]</sup>

1T MoS<sub>2</sub> nanosheets produced by LiBH<sub>4</sub> exfoliation have the lateral size up to 1  $\mu\text{m}$  and the 1T content  $>80\%$ .<sup>[25,63]</sup> When the 1T nanosheets were converted to 1H phase by annealing, the Tafel slope increased from 40 to 75–85 mV dec<sup>-1</sup> and the onset overpotential became higher. The high HER performance of 1T MoS<sub>2</sub> sheets was mainly owing to the low  $\Delta G_{H^*}$  at the basal plane (around 0.12 eV), closing to the  $\Delta G_{H^*}$  at the edge of 1H/2H MoS<sub>2</sub> (0.08 eV).<sup>[7,22–24]</sup>

Combining phase engineering and edge-enrichment, 1T MoS<sub>2</sub> monolayers with smaller sizes have also been prepared for HER. In 2017, Li et al. applied the intercalant of butyl lithium (*n*-butyllithium) to exfoliate MoS<sub>2</sub>.<sup>[64]</sup> With the assistance of ultrasonication treatment, the few-layered MoS<sub>2</sub> sheets was exfoliated, cracked, and converted to 1T MoS<sub>2</sub> nanosheets ( $>70\%$  phase content,  $\approx 100$ –200 nm in lateral size). The Tafel

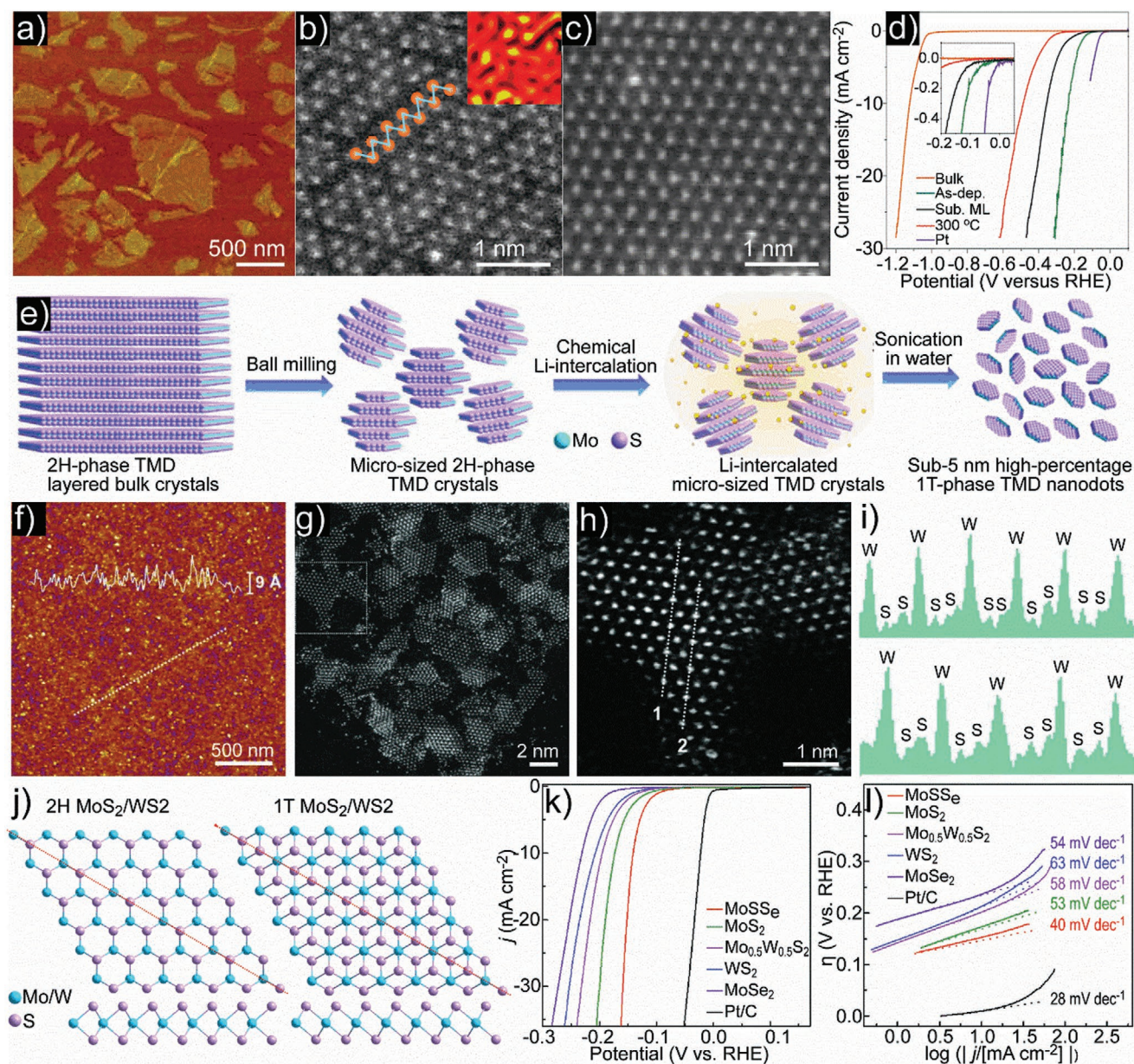


**Figure 3.** a) Atomic force microscopy (AFM) image of  $WS_2$  monolayers. High-angle annular dark-field scanning TEM (HAADF-STEM) images of the  $WS_2$  monolayer with distorted b) 1T and c) 1H structure. d) Polarization curves of bulk and  $WS_2$  monolayers (both 1T and 1H phases), sub-monolayered  $WS_2$  and Pt nanoparticles. (a–d) are reproduced with permission.<sup>[60]</sup> Copyright 2013, Springer Nature. e) Schematic shows the synthetic procedure of monolayered ultrasmall 1T TMDs from their 2H bulk crystals. f) AFM and g, h) HAADF-STEM images of the prepared monolayered  $WS_2$  NCs. h) The corresponding L2D-WF-ABSF filtered image of  $WS_2$  NCs in (g). i) Brightness profiles along the dotted lines in (h) (top, line 1; bottom, line 2). j) Schematic shows the structure of 1H/2H and 1T TMDs. k) Polarization curves and l) corresponding Tafel slopes of different monolayered NCs. (e–l) are reproduced with permission.<sup>[69]</sup> Copyright 2018, John Wiley & Sons.

slope and onset overpotential of the as-prepared 1T  $MoS_2$  nanosheets were  $42.7 \text{ mV dec}^{-1}$  and  $156 \text{ mV}$  respectively. This performance is worse than the above 1T  $MoS_2$  sheets due to the lower ratio of the 1T:1H phases and the fact that multilayered sheets were commonly found in the sample.<sup>[64]</sup> Nevertheless, the demonstrated performance is already dramatically improved from that of many 1H- $MoS_2$  monolayers.<sup>[10,62,65–67]</sup>

To expose the maximum surface active sites, He et al. proposed a solvothermal approach to preparing vertically aligned 1T

$WS_2$  sheets (phase content was around 70%) with a lateral size of several micrometers.<sup>[68]</sup> The vertically aligned 1T  $WS_2$  sheets exhibited a Tafel slope of  $43 \text{ mV dec}^{-1}$  and onset overpotential of  $118 \text{ mV}$  (at the  $j$  of  $10 \text{ mA cm}^{-2}$ ). By contrast, the flat 1T  $WS_2$  sheets on glassy carbon electrode has only the Tafel slope of  $52 \text{ mV dec}^{-1}$  and onset overpotential of  $230 \text{ mV}$ . Such an improvement is owing to the improved exposure of the 1T basal plane.

In 1T TMDs, the exposure of the basal plane becomes crucial to an efficient HER, which is different with that of most

**Table 1.** HER catalytic performance of various monolayered 1T-TMDs NCs.<sup>[69]</sup>

Parameters	MoS <sub>2</sub>	WS <sub>2</sub>	MoSe <sub>2</sub>	Mo <sub>0.5</sub> W <sub>0.5</sub> S <sub>2</sub>	MoSSe
Tafel Slope (mV dec <sup>-1</sup> )	53	63	54	58	40
Onset overpotential (mV)	58	139	101	95	49

1H/2H TMDs with only catalytically active edges. Monolayered 1T TMDs NCs have also been reported recently by Zhang and co-workers in 2018.<sup>[69]</sup> Bulk TMDs (size around tens of micrometers) were initially reduced to microsized particles (size around 1 μm) with ball-milling, and then intercalated by *n*-butyllithium producing various monolayered TMDs nanodots (MoS<sub>2</sub>, WS<sub>2</sub>, MoSe<sub>2</sub>, Mo<sub>0.5</sub>W<sub>0.5</sub>S<sub>2</sub>, and MoSSe) (sub-5 nm, Figure 3e–l) with a high percentage of 1T phase (67–80%). As

suggested in Figure 3k,l, the Tafel slope of these TMDs varies from 40 to 63 mV dec<sup>-1</sup>. The lowest Tafel slope was achieved on the MoSSe dots owing to possibly the Se-depleted sites formed during the preparation (see Table 1).<sup>[69]</sup> The Tafel slope of the 1T MoS<sub>2</sub> NCs was actually inferior to that of 1H monolayered NCs and 1T monolayered sheets,<sup>[10,67]</sup> and the underlying reason is still unclear (preparations and purifications of the 1T NCs may need to be improved further).

One important consideration of the phase engineering for TMDs is the confusion between 1T and 1T' phases which have dramatically different electronic properties and hence HER pathways. A recent work by Sokolikova et al.<sup>[26]</sup> demonstrated the solution phase synthesis of kinetically stabilized 1T' WSe<sub>2</sub> on arbitrary substrates (Figure 4). The Tafel slope of 1T' WSe<sub>2</sub> at ultralow mass loadings of 40 μg cm<sup>-2</sup> was 150 mV dec<sup>-1</sup> which increased dramatically to 232 mV dec<sup>-1</sup> upon the thermal

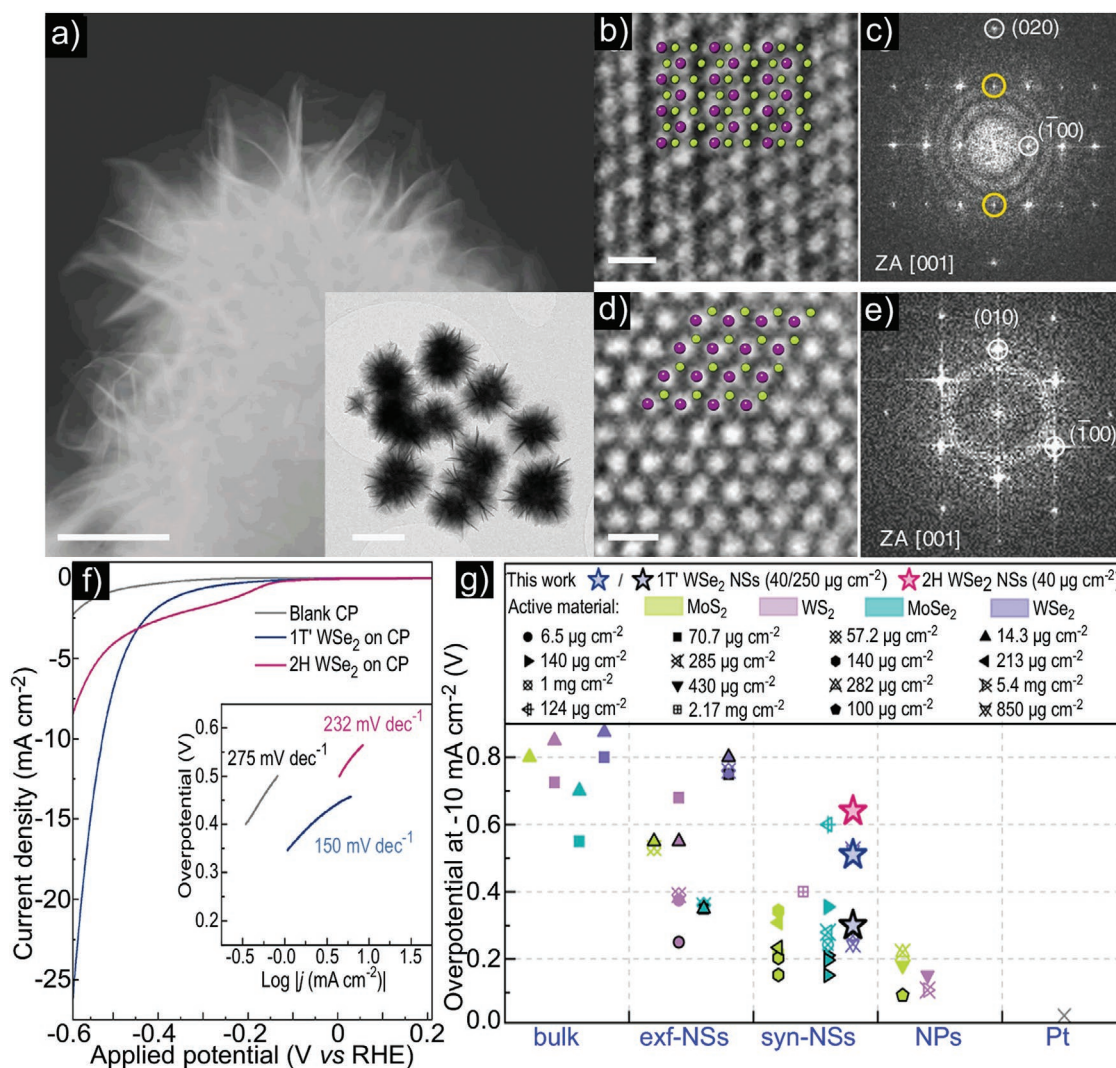


**Figure 4.** a) Annular dark-field scanning TEM image of a WSe<sub>2</sub> branched nanoflower illustrating ultrathin nature of individual nanosheets (scale bar: 100 nm), inset—an overview image of an ensemble of the WSe<sub>2</sub> nanoflowers (scale bar: 200 nm). b–d) Zoomed-in image (scale bar: 0.5 nm) with an overlaid crystal model of b) the 1T' and d) 2H. c,e) Fast Fourier transform (FFT). f) Polarization curves of the 1T' and 2H WSe<sub>2</sub> nanosheets grown on the carbon paper, inset shows corresponding Tafel slopes. g) Comparison plot summarizing the reported group VI TMD electrocatalysts for HER (exf-NSs, exfoliated nanosheets; syn-NSs, synthesized nanosheets; NPs, nanoparticles). (a–g) are reproduced with permission.<sup>[26]</sup> Copyright 2019, Springer Nature.

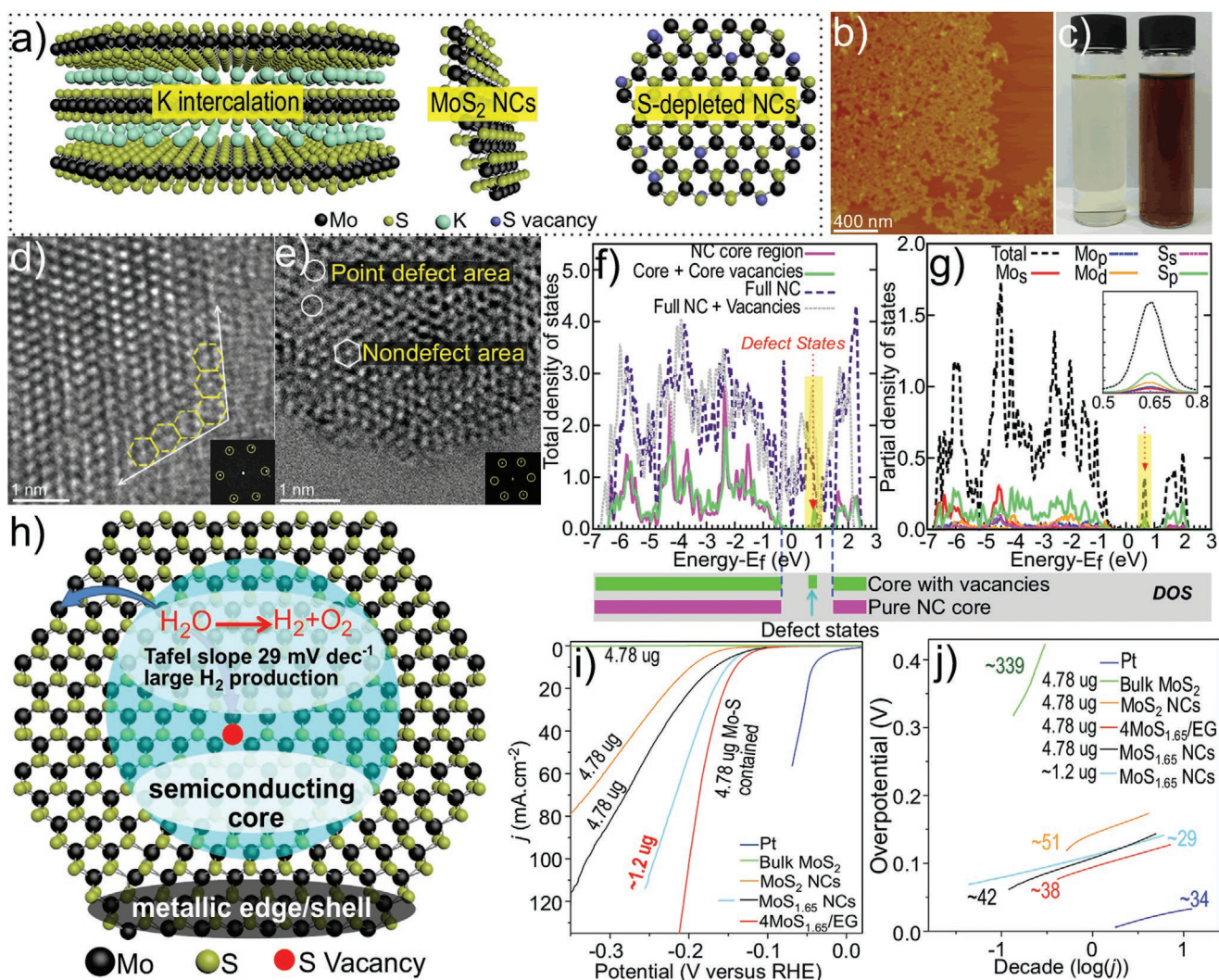


**Figure 5.** a) Schematic shows the preparation of monolayered MoS<sub>2</sub> NCs. Reproduced with permission.<sup>[71]</sup> Copyright 2017, Elsevier. b) The AFM image of the monolayered MoS<sub>2</sub> NCs. c) The optical image of the monolayered Mo-S NCs before (left) and after S-depletion (right). d) TEM images of the Mo-S NCs before S-depletion and e) TEM images of the Mo-S NCs after S-depletion. Insets are relating FFT patterns. f) Calculated density of state (DOS) of MoS<sub>2</sub> in the core and/or edge region, and the entire NC. g) Decomposition of the total DOS of MoS<sub>2</sub> in the core with S vacancies (S depletion) and edge regions into partial DOS of the Mo and S orbitals. h) Schematic shows the metallic edge, near-edge regions, and semiconducting core of the MoS<sub>2</sub> NCs. i) Polarization curves and j) Tafel plots of different catalysts in 0.5 M H<sub>2</sub>SO<sub>4</sub>. (b–j) are reproduced with permission.<sup>[10]</sup> Copyright 2016, American Chemical Society.

conversion to 1H/2H WSe<sub>2</sub> (Figure 4f). While the performance of the Tafel slope and the  $j$  at 10 mA cm<sup>-2</sup> were significantly improved from other optimized TMDs (Figure 4f,g), this approach shows the power of phase engineering to enhance catalysis when applied intelligently. To further improve the catalytic performance, additional approaches are also suggested, that will be further discussed below.

## 4.2. Defect Engineering

### 4.2.1. Size Control and Edge Enrichment

The catalytic activity of monolayers, in principle, can be rationally improved by the lateral size reduction to improve the

density of edge sites (Figure 2c). We developed a method to produce monolayered 1H MoS<sub>2</sub> NCs with a lateral size around 12.5 nm (Figure 5).<sup>[10,70]</sup> The Tafel slope and onset overpotential of the 1H MoS<sub>2</sub> NCs (on glassy carbon electrode) were 51 mV dec<sup>-1</sup> and 120–140 mV respectively (Figure 5i,j), which are clearly better than monolayered 1H MoS<sub>2</sub> sheets (on Au foil electrode),<sup>[62]</sup> and similar to the monolayered 1T WS<sub>2</sub> nanosheets (on glassy carbon electrode).<sup>[60]</sup> Theoretical calculations (Figure 5f,g) demonstrated that the 1H MoS<sub>2</sub> NC also have a metallic surrounding region that wraps the semiconducting core, improving the charge transport at the catalytically active sites.<sup>[10,71]</sup>

The formation of pores within larger monolayers can also enrich the catalytically active edge sites. Ajayan and co-workers has demonstrated this concept with 1H MoS<sub>2</sub>

monolayer triangles prepared from a CVD method.<sup>[72]</sup> These highly crystallized 1H monolayers were large in size (up to 100  $\mu\text{m}$ ), and nearly inactive for HER (Tafel slope of 342  $\text{mV dec}^{-1}$  and onset overpotential around 500 mV).<sup>[72]</sup> The samples were activated for HER by  $\text{O}_2$  plasma pore generation leading to a Tafel slope and onset overpotential of 162–171  $\text{mV dec}^{-1}$  and 400 mV, respectively. The newly formed inside edges consisted of both S and Mo terminated structures. Another strategy is annealing  $\text{MoS}_2$  monolayers with  $\text{H}_2$  to create pores/edges inside the monolayer. The Tafel slope and onset overpotential of these edge-rich monolayers were 117  $\text{mV dec}^{-1}$  and 300 mV, respectively. With smaller starting crystal sizes (100–200 nm), the HER performance can be improved further with a Tafel slope of 50  $\text{mV dec}^{-1}$  and onset overpotential of 120 mV.<sup>[65]</sup>

Ultrathin  $\text{TaS}_2$  sheets have also been treated by  $\text{O}_2$ -plasma to generate internal pores (Li et al. 2016).<sup>[73]</sup> The initial highly crystallized  $\text{TaS}_2$  sheets were created by chemical exfoliation, and have the lateral size about 15  $\mu\text{m}$  with a thickness of 1–3 layers.<sup>[73]</sup> After the pore generation, the Tafel slope and onset overpotential were both reduced from 215  $\text{mV dec}^{-1}$  and 310 mV, to 125–142  $\text{mV dec}^{-1}$  and 225 mV, respectively.<sup>[73]</sup>

Besides,  $\text{H}_2\text{O}_2$  oxidation can be combined with the traditional liquid exfoliation process for  $\text{MoSe}_2$  to introduce chemically induced pores.<sup>[74,75]</sup> During this process, the thin exfoliated  $\text{MoSe}_2$  sheets were oxidized and etched to generate pores with high density. While the Tafel slope (80  $\text{mV dec}^{-1}$ ) did not change significantly, the onset overpotential of the porous  $\text{MoSe}_2$  was greatly reduced to 75 from 220 mV by this pore generation process.<sup>[75]</sup>

Both edge-enrichment and creating monolayered NCs with small lateral size (e.g., 5–10 nm) are promising approaches, however, the small lateral size systems show better HER performance, even for the multilayered TMDs NCs with partial 1T phase.<sup>[69]</sup> With ongoing developments in synthesis techniques<sup>[10,69,71,76–79]</sup> the formation of the monolayered TMDs NCs is a highly promising strategy to achieve optimal HER catalytic performance. The edge enrichment and size control, at least, can be complimented with the phase engineering we have discussed above, although the stability of the 1T/1T' TMDs is still need to be appropriately addressed. Beyond this phase engineering, the following sections suggest that more strategies can be adapted together with the edge and size control, to further improve the HER performance.

#### 4.2.2. Defect and Strain Engineering

While phase engineering is a powerful tool to unlock catalytic potential for TMDs, there is significant value in exploring the optimization of thermodynamically stable 1H/2H TMDs for HER. A key consideration is that, as we have described previously, the basal plane of 1H/2H TMDs is relatively inactive for HER, and this contributes a huge amount of the surface area. By calculating the  $\Delta G_{\text{H}^*}$  during the Volmer reaction, Wang and co-workers suggested that various types of the S vacancies could activate the HER activity on the basal plane of  $\text{MoS}_2$ , with these new S-depleted sites being suited for both Tafel and Heyrovsky reactions.<sup>[80]</sup> Although precise control of these

S vacancies is still difficult, several reported literatures suggest that some favorable S vacancies could be formed on  $\text{MoS}_2$  monolayers.<sup>[81–85]</sup>

In 2016 the HER catalysis of the monolayered  $\text{MoS}_2$  NCs was studied (see Figure 5).<sup>[10]</sup> These fresh-prepared 1H  $\text{MoS}_2$  NCs (the lateral size around 12.5 nm) were treated with a cation exchange resin to gain S-depleted  $\text{MoS}_{1.65}$  NCs. The HER catalytic activity was highly improved from pure  $\text{MoS}_2$  NCs (Tafel slope of 51  $\text{mV dec}^{-1}$ , onset overpotential of 120–140 mV of pure NCs). These S-depleted NCs had a very low Tafel slope of 29  $\text{mV dec}^{-1}$ , low onset overpotential of 60–75 mV (extrapolated from the Tafel plot and the cathodic Tafel line), and high  $j_0$  of  $4.13 \times 10^{-3}$   $\text{mA cm}^{-2}$ .<sup>[10]</sup> The low Tafel slope around 30  $\text{mV dec}^{-1}$  suggested a Volmer–Tafel pathway reaction of the Mo-S NCs, which is highly promising and is among the best Mo-S base catalysts developed so far. Density functional theory (DFT) calculations showed addition effects of the defect generation including induced lattice strain, and new electronic states below the conduction band enhancing electron transport efficiency and promoting HER activity.

Controllable S-depletion and the relating HER catalytic activity should also be established to guide further improvements. In 2015, Zheng and co-workers systematically investigated the relationship between the point S-vacancies of  $\text{MoS}_2$  and the HER catalytic activity on the defected sites (Figure 6).<sup>[86]</sup> The calculated  $\Delta G_{\text{H}^*}$  on the basal plane without surface S-depletion is around 2 eV (catalytic insert for HER) which decreases to 0.18 eV with 3.12% surface S-depletion (Figure 6b), and reaches  $\pm 0.08$  eV with 9.38–18.75% S-vacancies. Fine control of the S-vacancies can generate more suitable  $\Delta G_{\text{H}^*}$  to thermos-neutral, which is better than that of the best configured edge sites. The  $\Delta G_{\text{H}^*}$  on the basal plane can also be tuned to be negative and close to 0 eV, giving better adsorption of the H atoms during the Volmer reaction (Figure 6b). Considering that the strain on the basal plane has also improved the HER catalytic performance owing to the strengthened hydrogen binding,<sup>[60,87]</sup> the  $\Delta G_{\text{H}^*}$  of the  $\text{MoS}_2$  monolayers with uniaxial elastic strain was further simulated. As suggested in Figure 6c, the  $\Delta G_{\text{H}^*}$  decreased with the strain for any investigated concentrations of the S-vacancy. This result is useful since the  $\text{MoS}_2$  monolayers are less stable with more S-vacancies, and the small applied strain could improve the stability with few S-depletions for the best HER. Modeled electronic structures showed that the S-depletion has introduced the defect level between the gap and under the bottom of the conduction band minimum.<sup>[71,86,88]</sup> In a n-type semiconductor such as 1H  $\text{MoS}_2$  monolayer, the Fermi level should close to the conduction band.<sup>[71,89]</sup> The hydrogen adsorption on the S-depleted Mo sites of the basal plane is induced by these newly formed gap states (localized around the S-vacancy). The bands move closer to the Fermi level (the number of gap states also increased) with more S-vacancies, which rationally explained the gradual improved H binding (Figure 6b,c). Tensile strain has also such effect to the gap states, and strengthened the hydrogen binding.<sup>[60,86,87]</sup>

Building on these theoretical understandings, Zheng and co-workers prepared large 1H  $\text{MoS}_2$  monolayer sheet with the minimized edge ratio.<sup>[86]</sup> Both strained ( $1.35 \pm 0.15\%$ ) and unstrained  $\text{MoS}_2$  monolayers were produced with

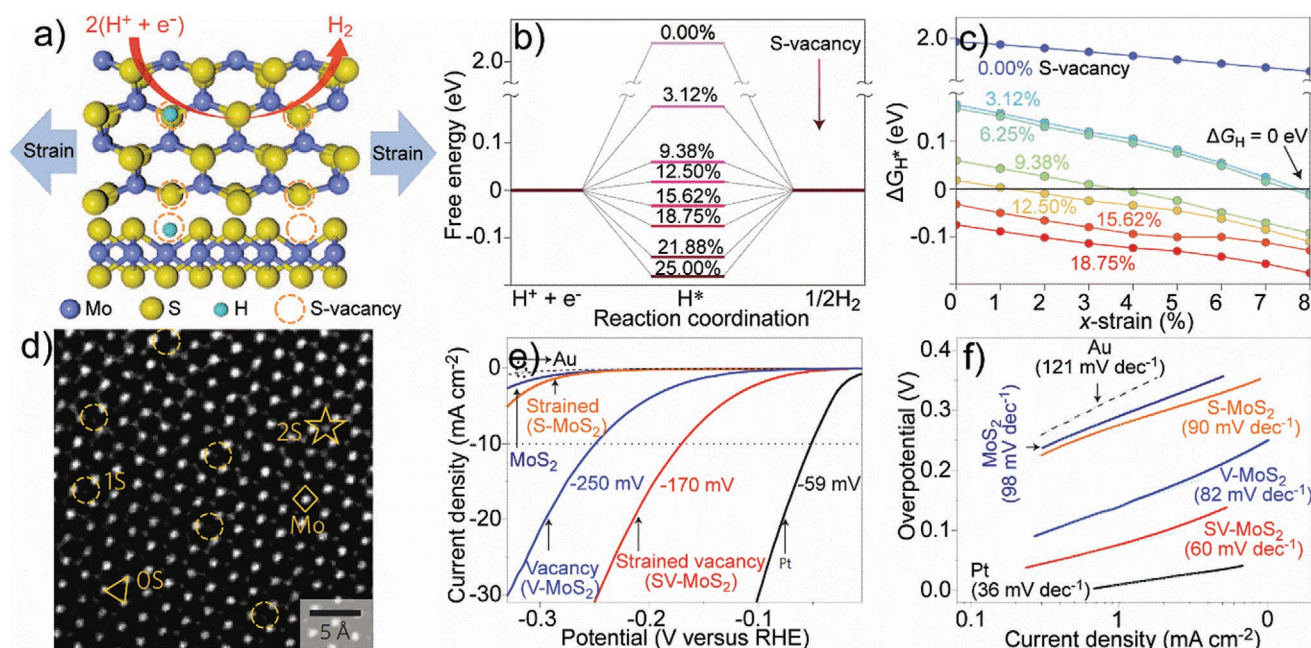


**Figure 6.** a) Schematic shows the top (top) and side (bottom) views of MoS<sub>2</sub> with strained S-vacancies on the basal plane. Theoretical calculations show b) the  $\Delta G_{H^*}$  versus the reaction coordination of HER upon the S-vacancies and c) the  $\Delta G_{H^*}$  versus the x-strain with S-vacancies. d) The aberration-corrected (AC) TEM image of MoS<sub>2</sub> monolayer (4 × 4 nm) with about 43 S-vacancies (≈11.3% S-vacancy) shows the Mo atoms, the pair of S atoms (2S, one S atom above the other below the Mo plane), the single S atoms (1S, only one S below the Mo plane) and the zero S atoms (0S, both the S atoms above and below the Mo plane were depleted). e, f) Polarization curves and Tafel slopes of different samples. S-MoS<sub>2</sub>, V-MoS<sub>2</sub>, and SV-MoS<sub>2</sub> are the MoS<sub>2</sub> monolayer with 0% S vacancy, 12.5 ± 2.5% S vacancies, and both the 1.35 ± 0.15% strain and 12.5 ± 2.5% S vacancies, respectively. (a–f) are reproduced with permission.<sup>[86]</sup> Copyright 2016, Springer Nature.

controlled S-vacancies (e.g., 21.88%, 18.75%, 12.50%, 8.00%, and 6.25%, to the total S atoms).<sup>[86]</sup> Theoretical calculations have further suggested that the strained (1.35 ± 0.15%) MoS<sub>2</sub> monolayer with 12.5% S vacancies has the best matched  $\Delta G_{H^*}$  to 0 eV.<sup>[86]</sup> The HER catalytic activity of the strained pure MoS<sub>2</sub> sheets was poor, with onset overpotential higher than 350 mV (determined by the current density at 10 mV cm<sup>-2</sup>) and Tafel slope of 90 mV dec<sup>-1</sup>. This HER performance was better than the pure MoS<sub>2</sub> without the strain (e.g., Tafel slope of 98 mV dec<sup>-1</sup>). Both the onset overpotential and Tafel slope of the MoS<sub>2</sub> monolayer were firstly reduced to 250 mV and 82 mV dec<sup>-1</sup> upon the S-depletion (12.5% S vacancies), which further reduced to 170 mV and 60 mV dec<sup>-1</sup>, respectively with additional 1.35 ± 0.15% strain (Figure 6e,f). The demonstrated best HER catalytic activity is below previously reported phase engineered and edge enriched TMDs,<sup>[51,60,67,90,91]</sup> but the performance improvement induced by the S-depletion and strain opens an attractive future pathway for HER optimization. As suggested in Figure 1e,f, the  $\Delta G_{H^*}$  on the basal plane of both 1H and 1T 2D-TMDs are all higher than 0 eV. Surface chalcogen vacancies could also improve the H binding and reduce the  $\Delta G_{H^*}$  to be more thermodynamically neutral. Such an improvement has already been demonstrated on the 2D MoSe<sub>2</sub> and MoSSe<sub>2</sub> NCs with Se vacancies.<sup>[69]</sup> Both the surface vacancies and strain have led to a decrease in the stability of TMDs, which restricted further exploitations of the strategy. To address this, other techniques such as surface doping can be introduced to stabilize the structure as well as to reach the optimized  $\Delta G_{H^*}$ .

### 4.3. Chemical Doping

The approaches discussed thus far have focused on manipulating the electrical properties and edge states of TMDs. However, more marked effects can be achieved by substituting either the transition metal or the chalcogen in a TMD structure, yielding new chemistries, band structures, and lattice strain toward optimized HER catalysis. Chemical doping of TMDs by various elements such as Pt, Co, Fe, Ni, O, Cl, and Se can effectively tune the electronic structure and improve the HER catalytic activity.<sup>[92–104]</sup> The external atoms could replace or bind with the M/X atoms on both the basal plane and edge of TMDs, depending on the reaction dynamics and the stability of the doped structure. Chemical doping could regulate the electronic structure of TMDs, resulting in high electrical conductivity.<sup>[105]</sup> The HER catalytic activity of TMDs could also be finely tailored by changing the  $\Delta G_{H^*}$  in the Volmer reaction and providing new active sites of the dopant itself.

#### 4.3.1. Doping with Metals

Among various doping approaches, the incorporation of a metal atom was frequently used to tune the  $\Delta G_{H^*}$ . For example, Tang and Jiang investigated the shift of the  $\Delta G_{H^*}$  of 1T MoS<sub>2</sub> by substitutional doping of the Mo site with different elements (V, Cr, Mn, Fe, Co, Ni, Nb, Ta, W, or Re), with DFT calculations.<sup>[12]</sup> The doping of Mn, Cr, Cu, Ni, and Fe all reduced the  $\Delta G_{H^*}$  in close to 0 eV. However, realization of such substitutional

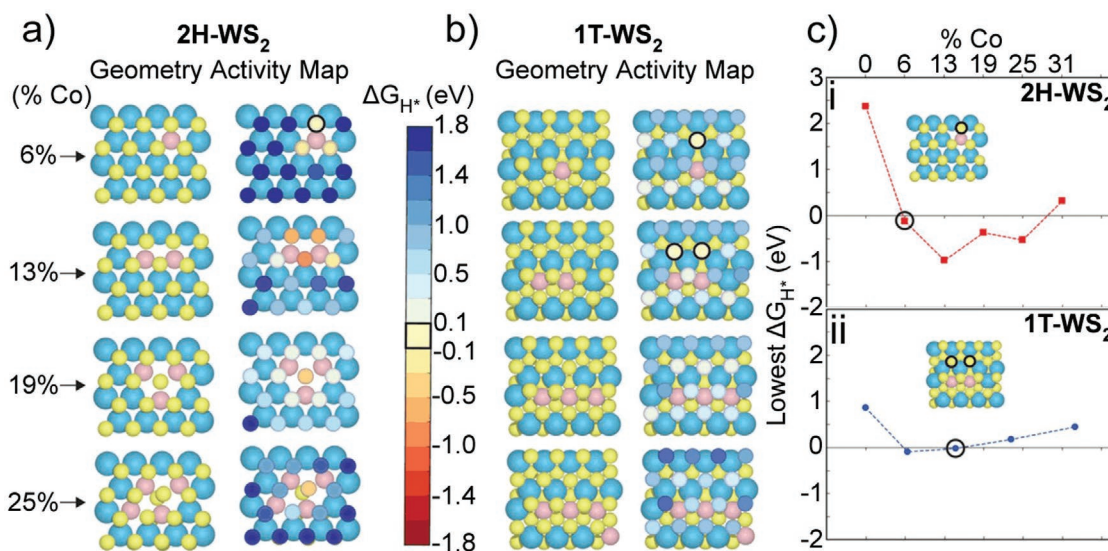


**Figure 7.**  $\Delta G_{H^*}$  of 2H and 1T WS<sub>2</sub> with increasing Co-dopant concentrations (W: turquoise; S: yellow; Co: light pink): a,b) Stable geometry (left) and activity map (right) as a function of Co doping concentrations. In the middle color scale bar, dark blue, red and yellow correspond to weak, strong and the optimal range for H adsorption. c) Plot of the minimum  $\Delta G_{H^*}$  across the basal plane of i) 2H-WS<sub>2</sub> and ii) 1T-WS<sub>2</sub> as a function of doping concentrations. (a–c) are reproduced with permission.<sup>[108]</sup> Copyright 2018, The Royal Society of Chemistry.

doping is challenging since the surface of 1T TMDs is highly reactive toward surface covalent functionalization and the surface of 2H/1H TMDs is relatively chemical inert.<sup>[106,107]</sup> Investigations have implied that the doping of MoS<sub>2</sub> is tend to be the functionalization on the active surface and the position at the S vacancy, resulting stable structures with different HER promotion effects.<sup>[106,107]</sup>

In 2012, Merki et al. demonstrated the doping of MoS<sub>2</sub> with various metals via electrochemistry.<sup>[92]</sup> They used the amorphous MoS<sub>3</sub> with rich edge sites to hold the dopants of Mn, Fe, Co, Ni, Cu, and Zn elements. The initial amorphous MoS<sub>3</sub> film has the onset overpotential of 171–203 mV,  $j_0$  of  $8.9 \times 10^{-4}$  mA cm<sup>-2</sup> and Tafel slope of 86 mV dec<sup>-1</sup> at pH = 7.<sup>[92]</sup> It was found that the Fe, Co, and Ni doping significantly improved the intrinsic activity of the catalyst under equilibrium conditions ( $j_0$ ) and the Mn, Cu, Zn doping showed slightly improvement on  $j_0$ . The  $\Delta G_{H^*}$  at the Mo- and S edges were calculated as 0.08 and 0.18 eV (associated with a single lowest energy site) respectively, basing on the model with the best H coverage. Incorporation of Co did not change the  $\Delta G_{H^*}$  at the Mo-edge, but lowered the  $\Delta G_{H^*}$  at the S-edge.

It is crucial to determine the optimal amount of dopants using DFT calculations as it highly affects the  $\Delta G_{H^*}$ . Zheng and co-workers investigated the  $\Delta G_{H^*}$  to understand the binding behavior of the whole surface of both 1H/2H and 1T WS<sub>2</sub> as a function of the concentration of substitutional Co dopants (calculation models are shown in Figure 7a,b, 4 × 4 unit cell).<sup>[108]</sup> Doping of Co with very high concentrations is thermodynamically unfavorable since the incorporation of Co into the WS<sub>2</sub> lattice is an endergonic process.<sup>[108]</sup> Similarly to the results reported by Merki et al.,<sup>[92]</sup> it was shown that the Co doping improves the HER catalytic activity by increasing the H adsorption on the S-sites neighboring the dopant.<sup>[108]</sup> The  $\Delta G_{H^*}$  of the plane site of 1H/2H WS<sub>2</sub> shift to increasingly orange exergonic values (−0.98 eV) with more Co

dopants (before 13% dopant), and then transit to increasingly blue endergonic values until the Co dopant's concentration of 25% (Figure 7). The optimized concentrations of Co doping on 1H/2H and 1T WS<sub>2</sub> are 6% (1 Co atom per unit cell) and 13% respectively, giving the best  $\Delta G_{H^*}$  at around −0.12 eV for the 1H/2H and −0.05 eV for the 1T WS<sub>2</sub>. Comparing with the pristine WS<sub>2</sub>, these two values are more suited for HER with higher catalytic activities (Figure 7c).

Other DFT calculations (summarized in Table 2) have also suggested the similar doping effect on the HER performance of TMDs, which agree well with some of experimental works.<sup>[12,93,99,108–112]</sup> Recently, Tsang and co-workers reported the Co and Ni doped thin MoS<sub>2</sub> nanosheets for HER.<sup>[113]</sup> They introduced Fe, Co, Ni, and Ag dopants into the structure of MoS<sub>2</sub> nanosheets (1–3 layers) via a solvothermal reaction.<sup>[113]</sup> Successful doping of the metal atoms have been confirmed by the HAADF-STEM observations. All these metal atoms can bind with the S atom, but only the Ni atom can also bind with Mo atoms to form metal–metal bond,<sup>[113]</sup> which is in consistent with the previous theoretical calculations.<sup>[109]</sup> The undoped thin MoS<sub>2</sub> nanosheets have an onset overpotential of around 300 mV (at the  $j$  of 10 mA cm<sup>-2</sup>) and Tafel slope of 94 mV dec<sup>-1</sup>. The Ag, Fe, and Ni doping have led to the larger onset overpotential, and the Co-doped MoS<sub>2</sub> showed much improved HER catalytic performance (onset overpotential at around 220 mV). Although the pristine and Co-doped MoS<sub>2</sub> all exhibited the Volmer–Heyrovsky pathway of the HER with similar Tafel slope ≈92–94 mV dec<sup>-1</sup>, the evidently lowered onset overpotential meant that the reaction barrier has been much alleviated. In 2017, Hu and co-workers also reported the improved HER on TMDs by Co doping.<sup>[114]</sup> They fabricated the 2D MoSe<sub>2</sub>/CoMoSe<sub>2</sub> heterostructures via a two-step CVD method with Co doping at the margin (edge). Onset overpotential (at the  $j$  of 10 mA cm<sup>-2</sup>) and Tafel slope of the doped heterostructures were 305 mV and 95.2 mV dec<sup>-1</sup>, respectively, greatly reduced

**Table 2.** Catalytic performance of doped TMDs. The best matched  $\Delta G_{H^*}$  of atoms near dopants or the active dopants was taken from literatures with suitable H coverage. X and M in this table are the chalcogen and the transition metal, respectively.

TMDs	Pristine $\Delta G_{H^*}$ [eV]			Dopants and Specification	$\Delta G_{H^*}$ [eV] after doping			Ref.
	Edge		Plane		Edge	Edge	Plane	
	X	M	X		X	M	X	
1H-MoS <sub>2</sub>	-0.45	0.06	-	Fe/Co/Cu (interstitially dope the S edge)	0.04/0.01/0.05	unaffected	-	[109]
				Ni (interstitially dope the Mo edge)	-0.08	0.15		
				Ni (interstitially dope the S edge)		-		
				Pt/Co/Ni/Ag/Zn/Pd/Au (replace Mo)	0.1/-/-/-/-/-	-	0/-0.07/-0.28/0.01/-0.05/-0.04/-0.07	[93]
			2.2	P (substitutional replace S)	Layer expanded		0.43 (0.04 at P sites)	[110]
		2.11	N (substitutional replace S)	Improved the electrical conductivity		0.71 (-1.43 at N sites)	[115]	
		-	O (substitutional replace S)		Improved the electrical conductivity		[105]	
1T-MoS <sub>2</sub>	-	-	0.13	Cr/Mn/Cu/Ni/Fe (replace Mo)	(W/Re/Nb/Ta/Co doping increase the $ \Delta G_{H^*} $ on the plane)		0.03/0.1/-0.07/-0.08/-1.2	[12]
1H-WS <sub>2</sub>	-	-	2.4	Co (replace 6% Mo atoms)	-	-	-0.12	[108]
1T-WS <sub>2</sub>	-	-	0.9	Co (replace 13% Mo atoms)	-	-	-0.05	[108]
1H MoSe <sub>2</sub>	0.51/0.28 (1/2 $H_{ads}$ )	0.08/-0.18 (1/2 $H_{ads}$ )	2.1	B replace Se atoms	-0.05/-0.12 (1/2 $H_{ads}$ )	-0.04/-0.24 (1/2 $H_{ads}$ )	1 (-0.15/-0.05 on the 1/2 B sites)	[111]
Ni <sub>2</sub> S <sub>3</sub>	S(100): 1.086, Ni(100): 0.583			N (replace S atoms)		-	0.036	[112]

from the 378 mV and 134 mV dec<sup>-1</sup> of the initial MoSe<sub>2</sub> sheets owing to the tuned  $\Delta G_{H^*}$  at the edge position.<sup>[114]</sup>

#### 4.3.2. Doping with Nonmetals

Besides the transition metals, the doping of nonmetals such as O, B, Cl, Se, P, N, and C have also been investigated to improve the catalytic performance on HER.<sup>[95,97-99,101,105,115]</sup> Theoretical calculations suggested that the P dopants (substitutional replace S, Table 2) can be the new active site ( $\Delta G_{H^*}$  of 0.04 eV) and offer the reduced  $\Delta G_{H^*}$  (0.43 eV vs 2.2 eV of pristine one) of the neighboring S atoms favoring for the HER.<sup>[110]</sup> The  $\Delta G_{H^*}$  can be further reduced to -0.11 eV by considering the layer expansion induced by the P dopant.<sup>[110]</sup> With controlled P doping, a Tafel slope of 34 mV dec<sup>-1</sup> and an extremely low onset overpotential of 43 mV was achieved for thin, layer expanded, MoS<sub>2</sub>.<sup>[110]</sup> Other measurements on the P doped 2D MoS<sub>2</sub> (also the WS<sub>2</sub>) have further confirmed the improved catalytic performance on HER.<sup>[99,116,117]</sup>

In 2017, Li et al. revealed that the N doping (through the substitution of S) can lead to the decrease of the  $\Delta G_{H^*}$  at the basal plane S atoms (0.71 eV vs 2.11 eV of pristine one, Table 2), while the N atom is inactive ( $\Delta G_{H^*}$  of -1.43 eV).<sup>[115]</sup> Although the  $\Delta G_{H^*}$  at the S atom is still high (0.71 eV), the N doped MoS<sub>2</sub> nanosheets showed a low Tafel slope of 45 mV dec<sup>-1</sup> and low

onset overpotential of 168 mV (at the  $j$  of 10 mA cm<sup>-2</sup>), which were largely improved from the pristine MoS<sub>2</sub>.<sup>[115]</sup> Unlike the P doped MoS<sub>2</sub>/WS<sub>2</sub> with significantly reduced  $\Delta G_{H^*}$ ,<sup>[110]</sup> the good catalytic performance on the HER of the N doped MoS<sub>2</sub> was also ascribed to the improved electrical conductivity upon the regulation of the electronic structure.<sup>[115]</sup> The increased density of the charge carrier has also been found in the O-doped MoS<sub>2</sub> sheets.<sup>[105]</sup> Other similar works have also demonstrated this improved electrical conductivity and the relating good HER performance of 2D TMDs.<sup>[98,101,118]</sup> Nevertheless, for different TMDs, the change of the  $\Delta G_{H^*}$  upon the N doping may be varied, i.e., the low  $\Delta G_{H^*}$  of 0.036 eV at the basal plane of Ni<sub>2</sub>S<sub>3</sub> (also named as TMDs in this report), which is more close to 0 eV comparing with that of the 1H edge of MoS<sub>2</sub>, WS<sub>2</sub>, and MoSSe (Table 2).<sup>[112]</sup>

Other nonmetal dopants such as B, Cl, Se, and C have also been investigated.<sup>[95,97,111,119]</sup> They can either tune the electronic structure to improve the electronic transport or tune the  $\Delta G_{H^*}$  for a better HER, i.e., the  $\Delta G_{H^*}$  of -0.05 eV at the plane B site of the B doped MoSe<sub>2</sub> sheet and the highly improved catalysis of the Cl doped MoS<sub>2</sub>.<sup>[95,111]</sup> With the same principle, using alternating layers of different chalcogen atoms within a single mono-layer TMD can also improve HER performance. In 2015, Ren et al. investigated the HER of the Se-doped MoS<sub>2</sub> nanosheets and presented a Tafel slope of 55 mV dec<sup>-1</sup> and an onset overpotential of 140 mV which were much improved

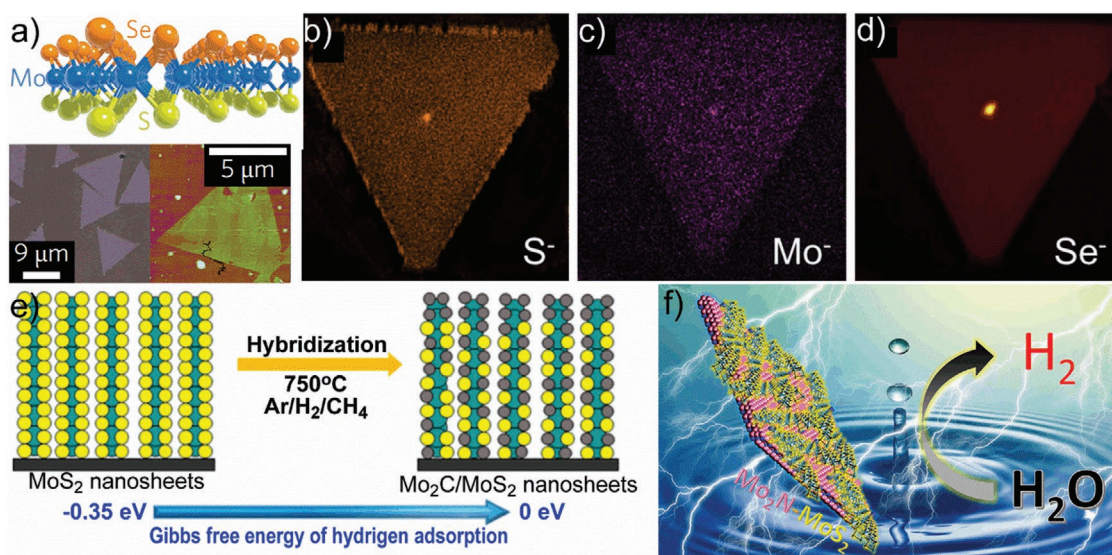


**Figure 8.** a) Schematic shows the Janus structure of S-Mo-Se triangular sheet (top) and corresponding optical (left bottom)/AFM (right bottom) images. Reproduced with permission.<sup>[122]</sup> Copyright 2017, Springer Nature. b–d) Time-of-flight secondary ion mass spectrometry (TOF-SIMS) of the Janus S-Mo-Se triangular sheet. Reproduced with permission.<sup>[120]</sup> Copyright 2017, American Chemical Society. e) Schematic of the Mo<sub>2</sub>C/MoS<sub>2</sub> hybrid nanosheets. Reproduced with permission.<sup>[127]</sup> Copyright 2017, American Chemical Society. f) Schematic of the HER on the hybrid structure of Mo<sub>2</sub>N and MoS<sub>2</sub>. Reproduced with permission.<sup>[128]</sup> Copyright 2019, American Chemical Society.

from the undoped MoS<sub>2</sub> nanosheets.<sup>[97]</sup> More careful preparations and experiments have been conducted on the Janus TMDs with controlled chalcogen substitution where one chalcogen layer is fully replaced by a different chalcogen.<sup>[120–126]</sup> One of the most studied version of these, the monolayered S-Mo-Se, can be considered as the MoS<sub>2</sub> monolayer with one Se substitutional doping layer (Figure 8a).<sup>[122]</sup> In the Janus structure, the breaking of structural symmetry gives large intrinsic lattice strain, and has significant effects in altering the band-structure for distinctive physical and chemical properties. The emergence of the in-gap states and the shift in the Fermi level of the Janus structure owing to the structure asymmetry largely effects the hydrogen adsorption.<sup>[123]</sup> Predictions have showed that the vacancy at the basal plane of the Janus S-W-Se monolayer is highly active for HER with the  $\Delta G_{H^*}$  (0.015 eV vs 0.18 eV of the plane of MoS<sub>2</sub> with S vacancy)<sup>[86]</sup> close to that of Pt, achieving the same result as through defect and strain engineering without sacrificing the structural stability.<sup>[123]</sup>

In 2017, Lou and co-workers prepared Janus S-Mo-Se monolayers (Figure 8b–d) via a CVD method.<sup>[120]</sup> Measurements on the patterned device (edges were covered to be inert) showed the HER performance of Se-Mo-S (S faces the substrate and Se is exposed for HER) > S-Mo-Se > MoSe<sub>2</sub>, were significantly improved compared to MoS<sub>2</sub>. The observed improvement in HER performance was ascribed to the presence of S or Se vacancies on the surface of the TMDs. The  $\Delta G_{H^*}$  on the plane was calculated as 0.007, 0.060, 0.063, 0.161 eV for Se-Mo-S (with single Se vacancy), S-Mo-Se (with single S vacancy), MoSe<sub>2</sub> (with single Se vacancy) and MoS<sub>2</sub> (with single S vacancy), respectively.<sup>[120]</sup> These results mean that the Janus Se-Mo-S is more promising than the MoS<sub>2</sub> monolayer, with fewer surface vacancies required for highly efficient and stable HER.

Although the experimental HER performance on Janus TMDs has not been well established (owing to the difficulty on

large scale fabrications), these results showed a promising path forward. The underlying mechanism for HER performance upon element doping and/or substitution can be used to guide further improvement of the HER catalytic performance. Nevertheless, comparing with NCs and nanosheets of some TMDs we discussed above, the doped TMDs actually have not showed outstanding catalytic performance. There are also several other factors which should be carefully addressed during the preparation of the catalyst electrode, such as the precise control of the doping and the clean surface of the TMDs after the doping treatment.

#### 4.4. Hybrid Structures

Unlike precise element doping, the fabrication of hybrid structures of TMDs and co-catalysts is more feasible. Systematic investigations suggested that the TMDs layer can be converted to other phases, i.e., the carbonization and nitridation of the MoS<sub>2</sub> to form MoC<sub>x</sub> and MoN<sub>x</sub>,<sup>[127–129]</sup> which have the outstanding catalytic performance on HER owing to the hybridization between the d-orbitals of Mo and the s- and p-orbitals of C/N, giving similar d-band electronic structure with Pt.<sup>[130–132]</sup> The synergistic effect (e.g., the improved charge injection from the co-catalyst) and the tuned  $\Delta G_{H^*}$  at the interface of the hybrid structure offer additional opportunities in improving the HER performance.<sup>[127,128]</sup> Recently, Zhao et al. fabricated the hybrid nanosheets (average thickness of 9 nm) of the MoS<sub>2</sub>/Mo<sub>2</sub>C (Figure 8e), with nanodomains of Mo<sub>2</sub>C or a mixture of S and C incorporated in the MoS<sub>2</sub> sheet.<sup>[127]</sup> DFT calculations suggested that some interfaces between the MoS<sub>2</sub> and Mo<sub>2</sub>C (Mo-S-C) have the  $\Delta G_{H^*}$  very close to 0 eV, giving the efficiently improved catalytic performance on HER (Tafel slope of 53 mV dec<sup>-1</sup>, and onset overpotential of 89 mV at *j* of 10 mA cm<sup>-2</sup>) over pure MoS<sub>2</sub> and Mo<sub>2</sub>C nanosheets.

Such positive effect of the interface is also applicable in various reported hybrid structures such as the MoS<sub>2</sub>/Mo<sub>2</sub>C on N doped carbon nanotubes (CNTs),<sup>[133]</sup> the WS<sub>2</sub>/W<sub>2</sub>C on N- and S-decorated carbon matrix,<sup>[134]</sup> the S-decorated Mo<sub>2</sub>C,<sup>[135]</sup> and the N, S co-doped Mo<sub>2</sub>C nanosheets.<sup>[136]</sup> According to the previous DFT calculations, the formation of the hybrid interface between multilayered TMDs (e.g., MoS<sub>2</sub>) and carbon materials is exothermic and favorable,<sup>[129]</sup> giving the tuned ΔG<sub>H\*</sub> to favor for the H adsorption/desorption, and the “ohmic contact” to low down the charge transfer resistance. This phenomenon explains well why the HER catalytic performance of some hybrid structures of TMDs and carbon materials, such as the MoSe<sub>2</sub> and CNTs,<sup>[137]</sup> the MoS<sub>2</sub>/MoSe<sub>2</sub> and graphene,<sup>[138,139]</sup> were significantly superior to their pure phases or mixtures.

As we have discussed above, TMDs and their carbides, hybrid structures of TMDs and their nitrides have also been investigated for the improved catalytic performance on HER. Such improvement has been demonstrated by a report of Ojha et al., where the Mo<sub>2</sub>N nanostructures conjugated with few-layer MoS<sub>2</sub> sheets on the surface were fabricated for HER (Figure 8f).<sup>[140]</sup> Ojha et al. then concluded that the interfaces and junctions between the Mo<sub>2</sub>N and MoS<sub>2</sub> contributed significantly in the promoted HER. Ang et al. explained that the boundary of Mo<sub>2</sub>N and MoS<sub>2</sub> generates the cleavage of H–O bond of the H<sub>3</sub>O<sup>+</sup> cation, resulting the improved H<sub>2</sub> generation.<sup>[136]</sup> Additional DFT calculations by Yang et al. showed an interfacial electric field between the Mo<sub>2</sub>N and MoS<sub>2</sub> domains, driving the force to facilitate the charge transfer for an efficient HER.<sup>[141]</sup> The charge transfer issue has also been considered in building other hybrid structures for the promoted HER, such as the Ag<sub>2</sub>S/MoS<sub>2</sub> and MoO<sub>2</sub>/MoS<sub>2</sub> nanocomposites.<sup>[142–144]</sup>

Further, other hybrid structures building on the TMDs have also been investigated to offer the multifunctions (e.g., both the HER and OER), which will be further examined in the following sections on the progress on the HER in alkaline electrolyte. Although the HER catalytic performance of these hybrid structures is still incomparable to other engineered 2D TMDs (e.g., edge enriched, phase engineered, NCs with surface vacancies), they have exhibited remarkable merits toward practical applications, that are the feasible fabrication, the low-cost, and the potential high robust structure. For example, these hybrid structures can be grown on the 3D robust support (e.g., carbon cloth, carbon paper and carbon foam) for direct use.<sup>[127,145]</sup>

#### 4.5. Strategies for the HER in the Alkaline Media

The catalytic reactions discussed above were mainly driven in the acid media. Nevertheless, the high potential of the overall water electrolysis is mainly raised from the sluggish four-electron transfer kinetic of the OER, which requires the alkaline media to accelerate the reaction. In this case, the adsorption of the OH<sup>−</sup> on the surface of TMDs (particularly the 2D phase) make them dispersible/soluble in the electrolyte.<sup>[71]</sup> Besides, the HER pathways in alkaline electrolytes (anode: 2OH<sup>−</sup> → H<sub>2</sub>O +  $\frac{1}{2}$ O<sub>2</sub> + 2e<sup>−</sup>; cathode: 2H<sub>2</sub>O + 2e<sup>−</sup> → H<sub>2</sub> + 2OH<sup>−</sup>) also changed from that in acidic conditions, and the OH<sup>−</sup>/H<sub>2</sub>O

adsorption/dissociation (rather the ΔG<sub>H\*</sub> alone) on the catalyst surface become crucial.<sup>[146–148]</sup>

The stabilization of TMDs on the electrode can be realized by direct binding with other robust support such as carbon fibers and carbon papers.<sup>[148–151]</sup> The key challenge of developing 2D TMDs for alkaline-based HER is how to improve the adsorption/dissociation of OH<sup>−</sup> and H<sub>2</sub>O molecules on the surface. Progress in this field suggested two main techniques, that are the chemical doping and the formation of a hybrid structure to tune the liquid/solid interface.<sup>[148–151]</sup> Recently, Zhang et al. reported the C doped MoS<sub>2</sub> (C-MoS<sub>2</sub>) sheets with exceptional capability of alkaline HER (1.0 M KOH), giving low Tafel slope of 46 mV dec<sup>−1</sup> and overpotential of 45 mV at 10 mA cm<sup>−2</sup> (vs 129 mV dec<sup>−1</sup> and 228 mV of pure MoS<sub>2</sub> sheets).<sup>[152]</sup> Such outstanding performance was ascribed to the change of the electronic and coordination structures of MoS<sub>2</sub> upon C doping (Figure 9a–c). Specifically, the C dopants prefer to form the sp<sup>2</sup> hybrid orbitals, vacating unhybridized 2p<sub>z</sub> orbitals perpendicular to the basal plane of MoS<sub>2</sub>. The perpendicular 2p<sub>z</sub> orbitals potentially offered active sites for water adsorption and activation, which was supported by the DFT calculations and absent in the case of pure MoS<sub>2</sub> (Figure 9a,b). The C dopants served as the site for H<sub>2</sub>O adsorption, and the nearby S sites assisted the water dissociation by attracting the H, resulting significantly lower potential energy for the water adsorption and dissociation on the surface of C-MoS<sub>2</sub> than that on the pure MoS<sub>2</sub> (Figure 9c), Mo<sub>2</sub>C and also S-depleted Mo-S sheets.<sup>[152]</sup>

With similar considerations of the electronic modulation, Huang et al. fabricated the metallic 1T MoS<sub>2</sub> with co-doping of O and Ni.<sup>[151]</sup> The doped 1T-MoS<sub>2</sub> has the hexagonal arrangement with the Ni center and surrounding Mo atoms (Figure 9d). This catalyst has a positive onset overpotential of ≈0 V and a low overpotential of 46 mV at *j* of 10 mA cm<sup>−2</sup> for the alkaline HER (1 M KOH), which is comparable to Pt-based catalyst.<sup>[151]</sup> DFT calculations suggested that all the Fe, Co, and Ni doping reduced the ΔG<sub>H\*</sub> at the basal plane of 1T MoS<sub>2</sub>, while the Ni doping has the best configurations (|ΔG<sub>H\*</sub>|). The ΔG(H<sub>2</sub>O) on the Ni doped 1T-MoS<sub>2</sub> is also reduced to 0.925 from 1.65 eV of pure 1T-MoS<sub>2</sub>, which is further reduced to 0.324 eV when O is introduced to form Ni-O-Mo configurations, benefiting the dissociation of H<sub>2</sub>O to H\* intermediates.<sup>[151]</sup>

Besides the doping strategies, formation of the hybrid structures has also been considered to offer multifunctions of the 2D TMD-based catalyst.<sup>[153]</sup> For example, Zheng and co-workers reported the hybrid structure of nickel hydr(oxy)oxide nanoparticles and the 1T MoS<sub>2</sub> nanosheets. The Ni-based nanoparticles were homogeneously loaded on the MoS<sub>2</sub> sheets (Figure 9e), facilitating the adsorption and dissociation of H<sub>2</sub>O, and supplying protons for subsequent HER reactions at nearby active sites on the 1T-MoS<sub>2</sub>. As a result of this “synergistic effect,” the hybrid catalyst showed a Tafel slope of 75 mV dec<sup>−1</sup> and the overpotential of 73 mV at 10 mA cm<sup>−2</sup> for alkaline HER (1 M KOH), which were greatly improved from the pristine 1T-MoS<sub>2</sub>. Similar “synergistic effect” has also been observed in many other reports.<sup>[148–150]</sup> In the work of Liu et al., Ru nanoparticles were loaded on the MoS<sub>2</sub>, giving the Tafel slope of 60 mV dec<sup>−1</sup> and the overpotential of 13 mV at 10 mA cm<sup>−2</sup> (1 M KOH, Figure 9f). In the acidic electrolyte, the improvement on the HER performance by the Ru nanoparticles was

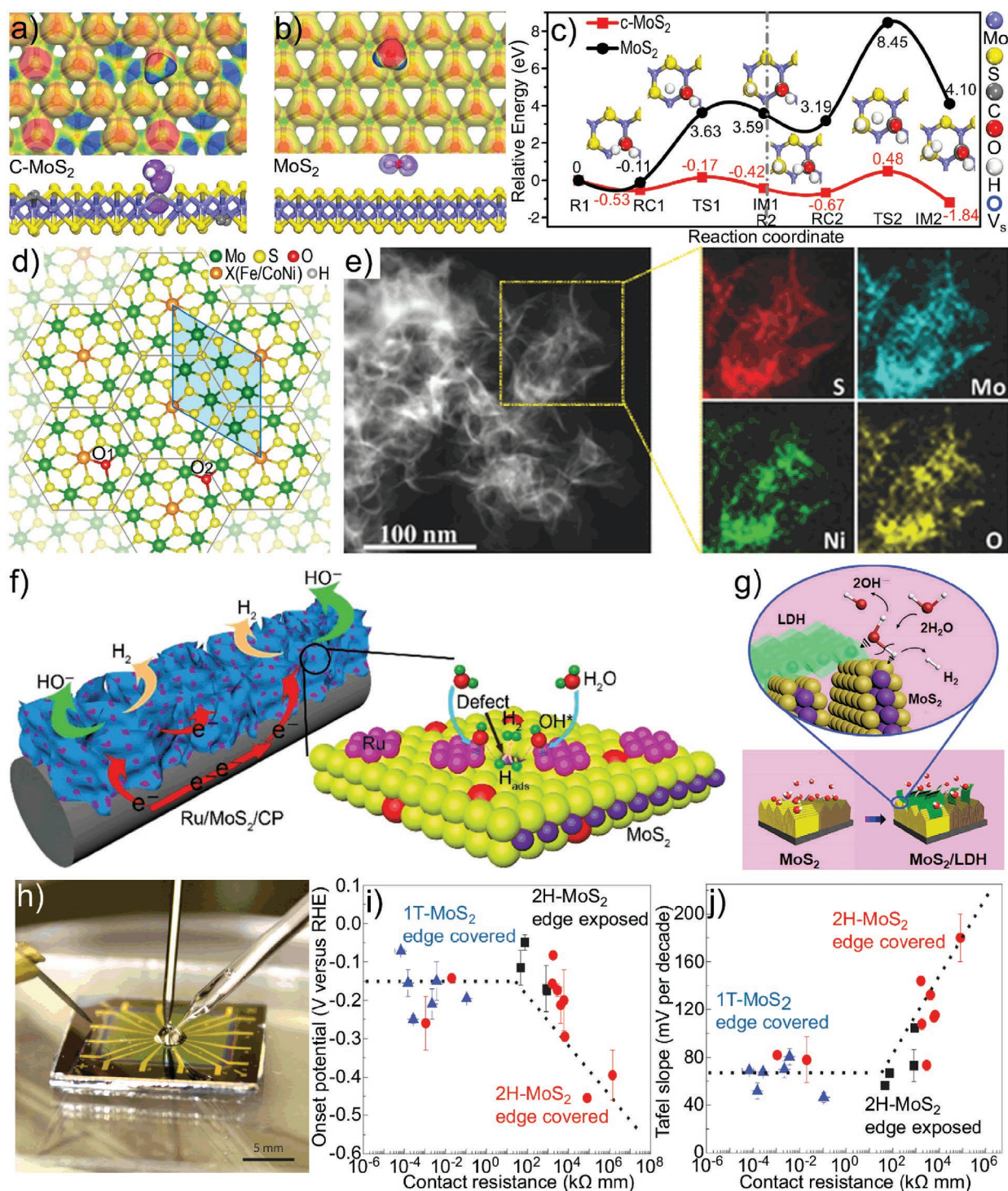


**Figure 9.** The top-view electrostatic potential of the water adsorbed on the basal plane, and the corresponding side-view bonding and nonbonding orbitals of a) C-MoS<sub>2</sub> and b) MoS<sub>2</sub>. c) The relative energy diagram along the reaction coordinate, including the first (left panel) and second (right panel) water dissociation process on the basal plane of MoS<sub>2</sub> and C-MoS<sub>2</sub>, respectively (R: reactant, RC: reactant complex, TS: transition state, IM: intermediate). (a–c) are reproduced with permission.<sup>[152]</sup> Copyright 2019, Springer Nature. d) The monolayer structure of XO@1T-MoS<sub>2</sub> (XO: metal heteroatom), showing the hexagonal XMo<sub>6</sub> units in XO-doped 1T-MoS<sub>2</sub> (X = Fe, Co, Ni). Reproduced with permission.<sup>[151]</sup> Copyright 2019, Springer Nature. e) HAADF-STEM and relating elemental mapping images of the 1T-MoS<sub>2</sub> nanosheets with Ni-based co-catalyst loaded on the surface. Reproduced with permission.<sup>[153]</sup> Copyright 2017, John Wiley & Sons. f) Schematic shows the interfacial synergy between Ru and MoS<sub>2</sub> for enhanced alkaline HER. Reproduced with permission.<sup>[148]</sup> Copyright 2017, Royal Society of Chemistry. g) Schematic shows the alkaline HER in the interface of MoS<sub>2</sub> and LDH. Reproduced with permission.<sup>[149]</sup> Copyright 2017, Elsevier. h) Photograph of the electrochemical microcell. i) Onset potential and j) Tafel slope of MoS<sub>2</sub> as a function of contact resistance. (h–j) are reproduced with permission.<sup>[154]</sup> Copyright 2016, Springer Nature.

neglectable and even worse since the OER was sluggish at low concentration of  $\text{OH}^-$ .<sup>[148]</sup> In 2017, Hu et al. reported the nano-hybridization of  $\text{MoS}_2$  with layered double hydroxides (NiCo-LDH), and demonstrated the Tafel slope of  $76.6 \text{ mV dec}^{-1}$  and overpotential of  $78 \text{ mV}$  at  $10 \text{ mA cm}^{-2}$  ( $1 \text{ M KOH}$ , Figure 9g).<sup>[149]</sup> This hybrid structure has the  $\text{MoS}_2$  core and the thin LDH outer layer (Figure 9g), where the LDH served as the acceptor of the  $\text{OH}^-$ . The above demonstrated “synergistic effect” suggests that many other OER catalysts can be rationally designed to bind with TMDs for an improved alkaline HER.

In hybrid structures, nevertheless, engineering TMDs still need to be considered to further improve the HER once the dissociation of  $\text{H}_2\text{O}$  (or the adsorption of the  $\text{OH}^-$ ) is secured by the co-catalyst in the interface of the hybrid structure. Comparisons between the doped and hybrid TMDs also suggested that the alkaline HER performance of the TMD-based hybrid structures are not outstanding; while the careful tune of the structure of 2D-TMDs (e.g., precise doping) is slightly difficult at this stage.

#### 4.6. Other Strategies and Factors

Beyond the fundamental manipulation of TMDs, there are several other pathways to control and engineer their HER performance, including electron transfer and substrate binding, intrinsic charge engineering, and the formation of TMDs heterostructures. Tsai et al. calculated the  $\Delta G_{\text{H}^*}$  at the edge of  $\text{MoS}_2$  nanosheets on different substrates, demonstrated that the best adhesion energy between  $\text{MoS}_2$  and the substrate should be  $-0.30 \text{ eV}$  for the optimal H adsorption.<sup>[24]</sup> On the other hand, charge transport between the electrode and the catalyst is important as it governs the Volmer and Heyrovsky reactions. Many 1H/2H TMDs are semiconductors with poor electrical conductivity, thus to drive the electrons to the active sites with additional electrical potential. This extra driving force can be minimized by size reduction, percolation, the addition of conductive fillers and intimate contact with a conductive substrate.

Intrinsic charge engineering is one strategy to consider this charge transport during the HER. It can facilitate electron injection from the electrode and transport to the catalyst by improving the electrical coupling between the substrate and the catalyst. Voiry et al. covered the edge of the  $\text{MoS}_2$  by polymethylmethacrylate (PMMA) for pure HER measurements on the basal plane (Figure 9h–j). They used phase engineering to locally tune the contact resistance,<sup>[154–156]</sup> demonstrating that both the Tafel slope and the onset overpotential of the basal plane of 2H/1T  $\text{MoS}_2$  nanosheets are highly depended on the contact resistance. Building on the improved charge injection on the basal plane and the existence of some S vacancies, the 2H  $\text{MoS}_2$  nanosheets exhibited the low Tafel slope of  $50 \text{ mV dec}^{-1}$  and low onset overpotential of  $100 \text{ mV}$ .<sup>[154]</sup> Besides this intrinsic charge engineering, improvement on the charge transport to tune the  $\Delta G_{\text{H}^*}$  has also been achieved via the TMDs heterostructures. For example, Vikraman et al. demonstrated the improved HER performance using  $\text{MoS}_2$ - $\text{WS}_2$  heterostructures owing to the elevation of electron–hole separation at the layer interfaces and sharing of active edge sites through the interface.<sup>[157]</sup> Kwon et al. have improved the HER catalytic

performance of  $\text{MoS}_2$  through the formation of n-TMD/p-TMD heterojunctions to use the high electric fields in the p–n junction.<sup>[158]</sup> Although the fabrication of these materials is not simple enough, the concept of the adhesion energy and charge injection can be well employed in building the hybrid structure that we have discussed above.

## 5. Comparison with other HER Catalysts

Our discussions suggest that 2D TMDs can be potentially well used in both acidic and alkaline HER. In recent years, several other state-of-the-art noble metal-free HER catalysts have also been developed, including alloys, heteroatom-doped carbon materials, metal phosphides, 2D metal oxides and MXenes (e.g., metal carbides and metal nitrides). In 2006, Nørskov and co-workers calculated the  $\Delta G_{\text{H}^*}$  of many pure metals and their bi-metallic alloys (Figure 10a), and suggested that many alloys are highly active for HER.<sup>[159]</sup> However, only a small fraction of these alloys were predicted being stable in acidic HER environments, including surface alloys of BiPt, PtRu, IrRe, and PtRh.<sup>[159]</sup> These stable catalysts are still expensive and unsuitable for large scale implementations. Other noble metal free alloys (e.g., NiMo) have also been reported being highly active in alkaline electrolyte, but their corrosion in acidic solution is still common.<sup>[160,161]</sup> Alloys with reduced cost (e.g., tri-metallic) and the monatomic/monolayered catalyst have also been reported,<sup>[162–165]</sup> which unfortunately still face either poor catalytic performance or challenging fabrication routes for large surface coverage (e.g., high loading of Pt on carbon support). In this regard, 2D TMDs exhibit significant advantages on the high exposure of the surface, which can be activated for both acidic and alkaline HER based on our discussions.

With the advantages of the low cost and easy fabrication, several heteroatom-doped carbon materials have been reported for HER in recent years, including N, O, S, and P doped carbon nanomaterials.<sup>[166–170]</sup> Nevertheless, the HER catalytic performance of these materials reported so far are still poor (most Tafel slopes were larger than  $100 \text{ mV dec}^{-1}$ ) comparing with that of 2D TMDs. Besides, like the alloy and heteroatom-doped carbon catalysts, several 2D TMDs are also highly conductive, i.e., the electrical conductivity of  $10\text{--}100 \text{ S cm}^{-1}$  of monolayered 1T  $\text{MoS}_2$  sheet at room temperature, comparable to the best-performing reduced graphene oxide sheet.<sup>[25]</sup> Even for the semiconducting 1H 2D TMDs, their poor charge transfer can be readily solved by intact contacting 2D TMD NCs onto the conductive substrate (e.g., the surface of 3D graphene).<sup>[171]</sup>

Like 2D TMDs, metal phosphides, such as  $\text{Co}_2\text{P}$ ,  $\text{MoP}$ , and  $\text{FeCoP}$ , have the  $|\Delta G_{\text{H}^*}|$  very close to  $0 \text{ eV}$  (Figure 10b).<sup>[172]</sup> They exhibited outstanding HER performance even superior to many 2D TMDs, i.e., the Tafel slope of  $33 \text{ mV dec}^{-1}$  and overpotential of  $23 \text{ mV}$  at  $j = 10 \text{ mA cm}^{-2}$  of the  $\text{Ni}_5\text{P}_4$  NCs (in  $0.5 \text{ M H}_2\text{SO}_4$ ),<sup>[173]</sup> and the Tafel slope of  $32 \text{ mV dec}^{-1}$  of  $\text{FeP}$  nanoparticles (in  $0.5 \text{ M H}_2\text{SO}_4$ ).<sup>[174]</sup> Some metal phosphides showed good alkaline HER performance, and also good oxidation resistance in both the acidic and alkaline electrolytes owing to relatively strong bonds between the metal and phosphide atoms.<sup>[173–176]</sup> Nevertheless, metal phosphides are typically non-layered materials which increases the materials usage in the

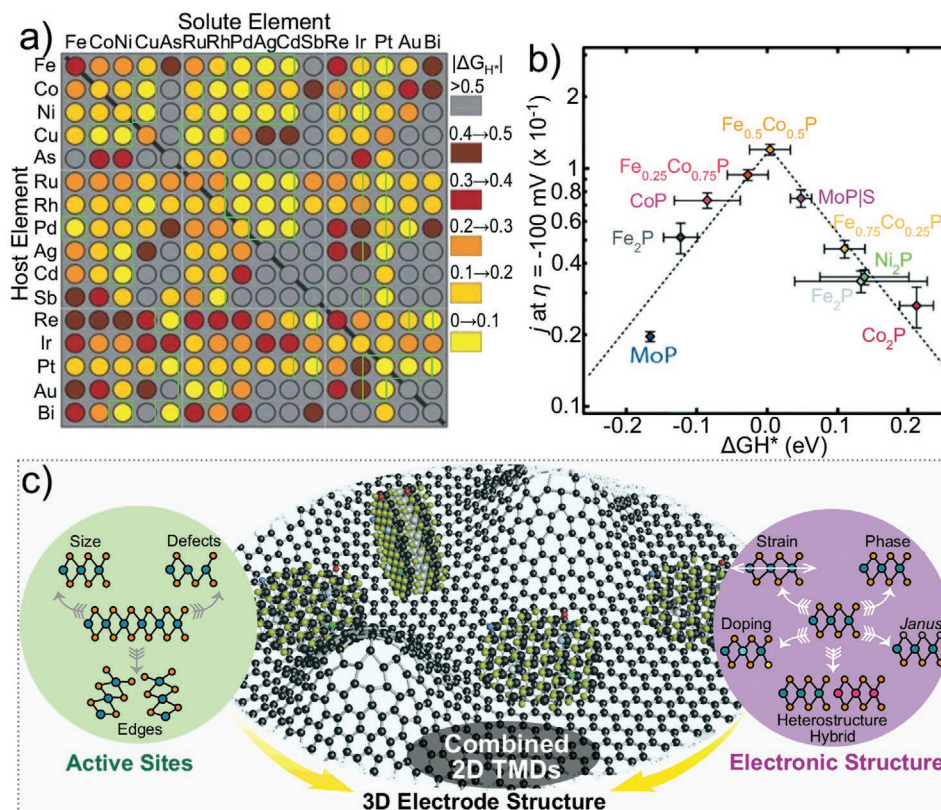


**Figure 10.** a)  $|\Delta G_{H^*}|$  on 256 pure metals and surface alloys. The rows indicate the pure metal substrates, and the columns indicate the solute embedded in the surface layer of the substrate (the solute coverage is 1/3 layer and the adsorbed hydrogen coverage is also 1/3 layer). Reproduced with permission.<sup>[159]</sup> Copyright 2019, Springer Nature. b) Activity volcano for the HER showing the electrochemical active surface area normalized current density from at  $\eta = 100$  mV as a function of  $\Delta G_{H^*}$ . Reproduced with permission.<sup>[172]</sup> Copyright 2015, Royal Society of Chemistry. c) Summary of the different approaches to optimizing TMDs HER catalytic activity by control of electronic structure and active sites in a 3D electrode, leading to a future where these can be synergistically applied to achieve cost-effective HER catalysis.

catalysis. The full exposure and participation of the surface and edges in the HER render particular advantages of 2D TMDs, although significant modifications of the materials (e.g., doping and hybrid structure) and relating engineering works of the electrode (e.g., 3D electrode) are still required to improve the HER performance.

Besides TMDs, many metal oxides and (oxy)hydroxides such as  $\text{V}_2\text{O}_5$  and  $\delta\text{-MnO}_2$  are also layered. Exfoliation of these materials can fully take the advantages of the high surface exposure for electrocatalysis. Although these 2D materials are highly promising in both the OER and oxygen reduction reaction (ORR), their HER performance are too poor to comparable with that of most advanced 2D TMDs.<sup>[177–179]</sup>

Other 2D layered materials beyond TMDs, the MXenes (e.g., metal carbides and metal nitrides), have also been investigated as outstanding HER catalyst. They have also very low  $\Delta G_{H^*}$  close to 0 eV, and sometimes performed better HER performance over the advanced 2D TMDs.<sup>[180]</sup> Differing from the active edge of 2D TMDs, the basal plane of many 2D MXenes (except the  $\text{Hf}_2\text{N}$ ,  $\text{V}_2\text{N}$ , and  $\text{W}_2\text{N}$ ) are HER active.<sup>[180]</sup> Nevertheless, the use of 2D MXenes in HER is highly stymied by their limited fabrication techniques, i.e., the fabrication of  $\text{Sc}_2\text{C}$  and  $\text{Hf}_2\text{N}$  which showed more optimized  $\Delta G_{H^*}$  than  $\text{Mo}_2\text{C}$ .<sup>[180]</sup> Even for the 2D  $\text{MoC}_2$ , their top-down fabrication normally

involve the selective etching process from their corresponding MAX phases with toxic fluoride chemicals,<sup>[180,181]</sup> while that of 2D TMDs are highly successful, including the CVD (as well as the epitaxial growth),<sup>[61]</sup> solvothermal synthesis,<sup>[182]</sup> liquid phase exfoliation,<sup>[74]</sup> chemical exfoliation,<sup>[60]</sup> tandem intercalation,<sup>[79]</sup> and the controlled explosion technique.<sup>[10]</sup> Nevertheless, taking both the advantages, and the “synergistic effected interface” (see Section 4.4) between these materials, the improved HER performance can be readily achieved by forming the hybrid structure of the 2D TMDs and MXenes.<sup>[127,128,136]</sup>

## 6. Conclusion and Prospect

TMD materials are highly promising as HER catalysts as they are relatively cheap, and highly tunable with phase-engineering, defect-engineering, chemical doping, hybrid and 3D structuring, as summarized in **Table 3**. These strategies all have both advantages and disadvantages, with the path forward utilizing a combination of these techniques. Ideally, a good HER catalyst for practical uses should have the following key features:

- A matched theoretical thermodynamic activity;
- A high density of catalytically active sites

**Table 3.** Comparison of various approaches for improving the HER catalytic activity of TMDs (mainly the MoS<sub>2</sub> as examples). In most literatures, a 0.5 M H<sub>2</sub>SO<sub>4</sub> electrolyte was used (pH value should not be equal to 0), and the  $j_0$  was usually affected by the amount of catalyst used in the test. We do not conclude these differences in the table.

TMDs	Strategy	Tafel slope [mV dec <sup>-1</sup> ]	$\eta$ [mV]	$j_0$ [mA cm <sup>-2</sup> ]	Stability (cycles/time)	Specification	Ref.
2H-MoS <sub>2</sub>	Nanoparticles (2 nm)	82–163	<160	–	Stable (1000)	Limited improvement, poor performance	[182]
MoS <sub>2</sub>	Amorphous	41–63 (1 M H <sub>2</sub> SO <sub>4</sub> )	–	10 <sup>-4.7</sup> –10 <sup>-3.2</sup>	Unstable (6)	Unstable catalytic performance	[38]
MoS <sub>2</sub>	Amorphous	40 (1 M H <sub>2</sub> SO <sub>4</sub> )	<170	1.3 × 10 <sup>-4</sup>	Unstable (18)		[39]
MoS <sub>2</sub>	Amorphous	29	0	5.6 × 10 <sup>-1</sup>	Unstable (1000)		[41]
2H-MoS <sub>2</sub>	Edge-aligned	86	–	2.2 × 10 <sup>-9</sup>	Stable (1000)	Promising, but the basal plane is inactive, edge can be enriched with small aligned sheets	[48]
2H-MoSe <sub>2</sub>	Edge-aligned	75	–	2.0 × 10 <sup>-9</sup>	Slight change (1000)		
2H-MoS <sub>2</sub>	Edge-aligned	36	119	–	Stable (1000)		[183]
2H-MoS <sub>2</sub>	Edge-aligned, interlayer expanded	56–73	133	0.56–0.93 × 10 <sup>-3</sup>	–		[51]
2H-MoS <sub>2</sub>	3D porous	50	<150	–	–	Edge exposed, charge transport is challenge	[52]
1H-MoS <sub>2</sub>	Monolayer sheet	75–85	–	–	–	Edge contribution is limited, inactive basal plane	[63]
1H-WSe <sub>2</sub>	Monolayer sheet	110	<150	–	–		[60]
1H-MoS <sub>2</sub>	Size reduced	51	<120	≈37 × 10 <sup>-3</sup>	–	Inactive basal plane	[10]
1T-MoS <sub>2</sub>	Phase change	40	–100	–	–	Promising, edge contribution limited or basal plane need to be further optimized	[63]
1T-WSe <sub>2</sub>	Monolayer sheet	55	<80	≈2 × 10 <sup>-2</sup>	Stable (10 000)		[60]
1T-MoS <sub>2</sub>	Edge-aligned, interlayer expanded, phase change	43–47	113	0.13–0.25 × 10 <sup>-3</sup>	Stable (1000)		[51]
1T-MoS <sub>2</sub>	Phase change and size reduction	53	58	–	–	Promising, performance can be further improved, fine control of the doping is challenge	[69]
1T-MoSSe	Phase change, size reduction and doping	40	49	–	–		
1H-MoS <sub>2</sub>	Size reduction and surface vacancy	29	<60	4.13 × 10 <sup>-3</sup>	Stable (3000)	Promising, need to be further improved	[10]
2H-MoS <sub>2</sub>	Doping, nanosheet	55	140	–	Stable (9000 s)	Promising, the basal plane is inactive, edge contribution is limited	[97]
1H-MoS <sub>2</sub>	Surface vacancy, strain	60	170	>10 <sup>-3</sup>	–	Conceptual promising, the demonstrated performance is poor, fabrication need to be further explored	[86]
2H-MoSe <sub>2</sub>	2D sheet, doping	95.2	305	–	Stable (12 h)	Conceptual promising, challenges in the fine control of the structure and doping.	[114]
1H/1T-MoS <sub>2</sub>	Electron injection, monolayer, few vacancies	40–50	50	1–17 × 10 <sup>-3</sup>	–		[154]
MoS <sub>2</sub> -WSe <sub>2</sub>	Heterostructure	72	129	4.36 × 10 <sup>-1</sup>	Stable (20 h)		[149]
1T' WSe <sub>2</sub>	Phase change	150	300	–	–	Low mass loadings	[26]

- iii) High electrical conductivity for efficient charge transport;
- iv) High stability; and
- v) Simple fabrication pathways, efficiency utilization of material uses for low cost manufacture.

It is still highly challenging to manufacture TMD based catalysts satisfying all these features. For example, owing to the abundant active sites adjacent to each other, amorphous MoS<sub>2</sub> film with outstanding catalytic activity comparable to that of

Pt has been demonstrated.<sup>[41]</sup> However, the catalyst durability of the film was too poor to support the practical use.<sup>[41]</sup> Some reported strategies for the TMD crystals with higher structure stability are more promising, but the demonstrated HER performance do not pass the threshold for commercial applications. Nevertheless, there are clear pathways forward to enable TMD catalysts for the efficient HER, and it is likely a combinational approach of size, defect, phase, hetero- and hybrid engineering, and coupled with electrode structuring to account for fluid and gas diffusion for the optimal performance of these materials.

In a structural view, a porous 3D electrode instead of the flat 2D substrate would be suggested. This electrode should have both the high electrical conductivity and good mechanical strength to bear the long-time impact of rapid H<sub>2</sub> bubble movement in the mass production of H<sub>2</sub>, i.e., the edge aligned nanosheets of TMDs (with expanded interlayer space) on the structural strengthened 3D graphene (or other similar supports). In this structure, edge ratio can be improved by reducing the lateral size, while the HER improvement from the interlayer expansion may be questionable since the mass diffusion and gas (bubble) release in such a small interlayer ( $\approx 1$  nm) is considerable poor comparing with that on the surface and edge exposing to the electrolyte directly. To expose the full surface, TMDs branches built by monolayered NCs on highly conductive stander like that of vertically aligned structure may be useful. Nevertheless, the formation of TMDs monolayer perpendicular to the 3D channel is highly challenging at the current stage. This structure also cannot promise the high mechanical strength of the active layer (e.g., desquamation from the substrate). With this consideration, the hybrid edge aligned nanosheets with thin TMDs layers outside the electrically conductive layers (Figure 10c) may be more promising. The TMD nanodomains could also hybrid with the conductive part at the outermost layer to improve the charge injection efficiency to the catalytically active site (Figure 10c). Fabrication of this hybrid structure is accessible, for example, the insufficient and controlled sulfuration of the monoclinic MoO<sub>2</sub> (metallic) sheets. The above structures on the 3D support may be too ambitious, and the structure on the surface of alternative mechanical robust and electrically conductive support (e.g., the carbon cloth) can be used (Figure 10c). Alternatively, to alleviate the negative effects from the electron hopping between multilayers and give more exposed active sites, rationally designed monolayered TMDs NCs (e.g., with high density of the active site, low  $E_a$  and suitable  $\Delta G_{H^*}$ ) could also layer-by-layer stacked with the internal channel of the 3D electrode (Figure 10c), if the interaction to the conductive substrate can be finely tuned for more efficient charge transport and the best matched  $\Delta G_{H^*}$ . In many reported literatures, 3D graphene have been frequently used to build HER catalyst owing to the large pore size and high electrical conductivity. Some functionalized 3D-G materials have the improved mechanical strength, while the electrical conductivities were normally degenerated.<sup>[184,185]</sup> Functionalization of the 3D-G with conducting polymer is also difficult in this case when the molecular of these conducting polymers are generally rigid (e.g., pyrrole). Rare works have been conducted to improve the mechanical strength, toughness and maintain the good electrical conductivity of such kind catalyst supports for

efficient HER. The influence of these catalyst supports on the catalytic performance is still need to be well established.

Building on the rationally designed structure of the electrode, the active part of the catalyst then can be further modified to follow the discussed strategies or their combinations (Figure 10c). Specifically, the activation of the surface could be realized by both the phase change and the surface vacancy/doping. As for the metallic 1T TMD monolayers reported so far, the demonstrated HER catalytic performance was actually not so good as expected.<sup>[22–24,63,64]</sup> More significantly improved HER performance was achieved on their small NCs (e.g., sub-5 nm).<sup>[69]</sup> Nevertheless, the Tafel slopes of these 1T TMD NCs ( $\approx 40$  mV dec<sup>-1</sup>, according to the slow Heyrovsky reaction) are still higher than the 29 mV dec<sup>-1</sup> of the S-depleted 1H MoS<sub>2</sub> NCs ( $\approx 12.5$  nm) and amorphous MoS<sub>2</sub>,<sup>[10,41]</sup> due to likely the still high  $\Delta G_{H^*}$  (e.g., 0.12 eV of MoS<sub>2</sub> monolayers) on the basal plane and the low ratio of the 1T monolayers in those as-prepared samples. Activation of the Tafel dominated reaction may need more adjacent active sites on the surface or the tuned reaction barriers by forming both the surface vacancy and doping. Improving the 1T ratio in a preparation may be realizable by taking the repeatedly and controlled insertion reaction with Li/Li<sup>+</sup> based on the small size and strong diffusion ability of the Li/Li<sup>+</sup> (repeat diffusion and insertion into the structure of TMDs to form a metastable phase), though it needs to be experimentally confirmed. Besides, the 1T TMDs are principally unsuitable for long-term operation due to the metastable nature. In this point, precise single-atom doping of the TMD can be considered as a pathway to adjust the structure stability, while the dopants can also serve as the highly active sites.<sup>[186,187]</sup> Although DFT calculations suggested that the some types of the doping, in particular the precious metals, on the pure TMDs (Table 2) are difficult,<sup>[93,108,109]</sup> the progress on the chalcogen-depletion of TMDs offers more possibility,<sup>[10,83–86]</sup> i.e., the stabilization of the Pt atoms on the chalcogen vacancy. More theoretical modeling is therefore highly anticipated to assist understanding the catalysis and the stability associated with these doping modifications. Although 1H S-depleted MoS<sub>2</sub> NCs were believed having metallic feature from theoretical calculations,<sup>[10,71]</sup> their 1T counterparts are still considered more promising. Nevertheless, further modifications of the 1H monolayered TMDs NCs may be necessary, if the phase stability of 1T TMDs cannot be well addressed. While the precise estimation of the catalytic activity is highly success with some conceptual devices,<sup>[154,188]</sup> development of the direct evaluation of the catalyst's stability is slightly behind. Upon the chemical doping at the atomic-level, the slight change of the catalyst may not be detectable by the frequently used "long-term" (e.g., hours or days) polarization curves of the power samples and ex situ characterizations. Other in situ observations of the catalyst may need to be involved by integration with the conceptual device, such as the electrochemical scanning tunneling microscope (ECSTM),<sup>[189]</sup> the scanning transmission electron microscopy (STEM),<sup>[190]</sup> the tip-enhanced Raman-SPM/AFM (SPM: scanning Probe Microscopy) combined microscopy and beyond.<sup>[191]</sup>

To tune the HER catalytic performance of TMDs, other techniques such as the formation of Janus structure, the creation of heterostructures and the interaction control between the TMDs and substrate would be also considered, though some preparations are still not feasible and cost-effective. These preparations

would be more complex in practical cases when more than one sensitive factors are involved to tune the catalytic performance. Another powerful aspect of TMD catalysis that can be used in complement to the techniques we have discussed is the fabrication of chemically functionalized TMDs, these functionalities can include noble metals as we have discussed above, and also the metal organic frameworks, layered perovskites, hybrid structures or organic group functionalization.<sup>[156–158,192–196]</sup> This is an emerging a powerful field as it opens a whole new set of possibilities to activate the catalytically active sites of TMDs and add catalytic activity, via the functional moiety, to inactive sites on the pristine TMD for both acidic and alkaline HER. Since heterostructuring is hugely flexible owing to van der Waals stacking, unique electronic band structures (e.g., tune the  $\Delta G_{H^*}$  and enable improved charge injection between interfaces) can be fabricated and tested in an extremely simple and controllable manner.<sup>[127,128,133–136]</sup> Together with some doping strategies, it also supports the alkaline HER of TMDs based materials.<sup>[156–158]</sup> While heterostructuring will need to be supported by robust DFT calculations.<sup>[197]</sup> It unlocks a plethora of potential material combinations and a whole new field of potential HER catalysts. While TMD heterostructures for electrocatalysis are only few and far between,<sup>[149,150]</sup> recent reports on improved synthesis techniques for photocatalysis show the promise and power of this approach.<sup>[197–200]</sup> On the catalytic activity scale, the emerging twistrionics may be introduced to precisely control the electronic structure of TMD bilayer heterostructures, where just by changing the angle of stacking significantly changes in band-structure emerge.<sup>[201,202]</sup> As studied between a wider variety of TMDs or incorporated into machine learning theory,<sup>[203,204]</sup> it is anticipated to be another powerful tool for optimized HER catalysis.

Therefore, building on the rational design of the electrode structure, and combining all of the techniques described above, TMDs can be highly promising catalysts to replace precious metals in efficient electrochemical HER (Figure 10c). This can be realized by building on more experimental and theoretical investigations on both TMDs and catalyst supports, as well as complementary 3D spatial electrode design.

## Acknowledgements

Funding from the Australian Research Council (CE 140100012, DP170102320 and DP170102267) and UOW VC Fellowship is gratefully acknowledged. The authors would like to thank the Australian National Fabrication Facility—Materials node for facility access.

## Conflict of Interest

The authors declare no conflict of interest.

## Keywords

2D materials, catalysis, energy conversion, hydrogen evolution reaction, transition metal dichalcogenides

Received: November 25, 2019  
Revised: February 2, 2020  
Published online: March 4, 2020

- [1] W. A. Braff, J. M. Mueller, J. E. Trancik, *Nat. Clim. Change* **2016**, 6, 964.
- [2] I. Dincer, *Int. J. Hydrogen Energy* **2012**, 37, 1954.
- [3] P. Nikolaidis, A. Poullikkas, *Renewable Sustainable Energy Rev.* **2017**, 67, 597.
- [4] L.-C. Ma, B. Castro-Dominguez, N. K. Kazantzis, Y. H. Ma, *Int. J. Greenh. Gas Control* **2015**, 42, 424.
- [5] M. S. Dresselhaus, I. L. Thomas, *Nature* **2001**, 414, 332.
- [6] J. A. Turner, *Science* **2004**, 305, 972.
- [7] B. Hinnemann, P. G. Moses, J. Bonde, K. P. Jørgensen, J. H. Nielsen, S. Horch, I. Chorkendorff, J. K. Nørskov, *J. Am. Chem. Soc.* **2005**, 127, 5308.
- [8] T. F. Jaramillo, K. P. Jørgensen, J. Bonde, J. H. Nielsen, S. Horch, I. Chorkendorff, *Science* **2007**, 317, 100.
- [9] Y. Yu, S.-Y. Huang, Y. Li, S. N. Steinmann, W. Yang, L. Cao, *Nano Lett.* **2014**, 14, 553.
- [10] L. Lin, N. Miao, Y. Wen, S. Zhang, P. Ghosez, Z. Sun, D. A. Allwood, *ACS Nano* **2016**, 10, 8929.
- [11] H. Helmholz, *Ann. Phys. Chem.* **1853**, 165, 353.
- [12] Q. Tang, D. Jiang, *ACS Catal.* **2016**, 6, 4953.
- [13] E. Skúlason, G. S. Karlberg, J. Rossmeisl, T. Bligaard, J. Greeley, H. Jónsson, J. K. Nørskov, *Phys. Chem. Chem. Phys.* **2007**, 9, 3241.
- [14] J. Rossmeisl, E. Skúlason, M. E. Bjorketun, V. Tripkovic, J. K. Nørskov, *Chem. Phys. Lett.* **2008**, 466, 68.
- [15] E. Skúlason, V. Tripkovic, M. E. Bjorketun, S. Gudmundsdottir, G. Karlberg, J. Rossmeisl, T. Bligaard, H. Jónsson, J. K. Nørskov, *J. Phys. Chem. C* **2010**, 114, 18182.
- [16] J. O. Bockris, E. C. Potter, *J. Electrochem. Soc.* **1952**, 99, 169.
- [17] B. E. Conway, B. V. Tilak, *Electrochim. Acta* **2002**, 47, 3571.
- [18] Y. Zhou, S. Xu, L. Guo, S. Zhang, H. Lu, Y. Gong, F. Gao, *RSC Adv.* **2015**, 5, 14804.
- [19] J. K. Nørskov, T. Bligaard, A. Logadottir, J. R. Kitchin, J. G. Chen, S. Pandelov, U. Stimming, *J. Electrochem. Soc.* **2005**, 152, J23.
- [20] H. I. Karunadasa, E. Montalvo, Y. Sun, M. Majda, J. R. Long, C. J. Chang, *Science* **2012**, 335, 698.
- [21] M. Chhowalla, H. S. Shin, G. Eda, L.-J. Li, K. P. Loh, H. Zhang, *Nat. Chem.* **2013**, 5, 263.
- [22] C. Tsai, K. Chan, F. Abild-Pedersen, J. K. Nørskov, *Phys. Chem. Chem. Phys.* **2014**, 16, 13156.
- [23] C. Tsai, F. Abild-Pedersen, J. K. Nørskov, *Nano Lett.* **2014**, 14, 1381.
- [24] C. Tsai, K. Chan, J. K. Nørskov, F. Abild-Pedersen, *Surf. Sci.* **2015**, 640, 133.
- [25] M. Acerce, D. Voiry, M. Chhowalla, *Nat. Nanotechnol.* **2015**, 10, 313.
- [26] M. S. Sokolikova, P. C. Sherrell, P. Palczynski, V. L. Bemmer, C. Mattevi, *Nat. Commun.* **2019**, 10, 712.
- [27] H. Tributsch, *Am. J. Phys. Sci.* **1977**, 32, 972.
- [28] V. Nicolosi, M. Chhowalla, M. G. Kanatzidis, M. S. Strano, J. N. Coleman, *Science* **2013**, 340, 1226419.
- [29] F. Reale, P. Palczynski, I. Amit, G. F. Jones, J. D. Mehew, A. Bacon, N. Ni, P. C. Sherrell, S. Agnoli, M. F. Craciun, S. Russo, C. Mattevi, *Sci. Rep.* **2017**, 7, 14911.
- [30] Y. H. Lee, X. Q. Zhang, W. Zhang, M. T. Chang, C. Te Lin, K. Di Chang, Y. C. Yu, J. T. W. Wang, C. S. Chang, L. J. Li, T. W. Lin, *Adv. Mater.* **2012**, 24, 2320.
- [31] Y. Li, K. A. N. Duerloo, K. Wauson, E. J. Reed, *Nat. Commun.* **2016**, 7, 10671.
- [32] X. Zhang, Z. Lai, Q. Ma, H. Zhang, *Chem. Soc. Rev.* **2018**, 47, 3301.
- [33] V. W. Lau, A. F. Masters, A. M. Bond, T. Maschmeyer, *Chem. - Eur. J.* **2012**, 18, 8230.
- [34] S. Fletcher, *J. Solid State Electrochem.* **2009**, 13, 537.
- [35] A. J. Appleby, J. H. Zagal, *J. Solid State Electrochem.* **2011**, 15, 1811.
- [36] J. Bonde, P. G. Moses, T. F. Jaramillo, J. K. Nørskov, I. Chorkendorff, *Faraday Discuss.* **2009**, 140, 219.

- [37] T. Wang, D. Gao, J. Zhou, Z. Zhu, P. Papakonstantinou, Y. Li, M. Li, *Chem. - Eur. J.* **2013**, *19*, 11939.
- [38] H. Vruble, D. Merki, X. Hu, *Energy Environ. Sci.* **2012**, *5*, 6136.
- [39] D. Merki, S. Fierro, H. Vruble, X. Hu, *Chem. Sci.* **2011**, *2*, 1262.
- [40] X. Ge, L. Chen, L. Zhang, Y. Wen, A. Hirata, M. Chen, *Adv. Mater.* **2014**, *26*, 3100.
- [41] T. Wang, J. Zhuo, K. Du, B. Chen, Z. Zhu, Y. Shao, M. Li, *Adv. Mater.* **2014**, *26*, 3761.
- [42] S. Cho, S. J. Kim, Y. Lee, J.-S. Kim, W.-B. Jung, H.-W. Yoo, H. Kim, H.-T. Jung, *ACS Nano* **2015**, *9*, 9314.
- [43] G. Deokar, P. Vancsó, R. Arenal, F. Ravoux, J. Casanova-Cháfer, E. Llober, A. Makarova, D. Vyalikh, C. Struzzi, P. Lambin, M. Jouiad, J. F. Colomer, *Adv. Mater. Interfaces* **2017**, *4*, 1700801.
- [44] C. Ma, X. Qi, B. Chen, S. Bao, Z. Yin, X. Wu, Z. Luo, J. Wei, H. Zhang, H. Zhang, *Nanoscale* **2014**, *6*, 5624.
- [45] J. Wang, D. Chao, J. Liu, L. Li, L. Lai, J. Lin, Z. Shen, *Nano Energy* **2014**, *7*, 151.
- [46] H. Bian, Y. Ju, J. Yan, P. Li, Y. Li, S. Liu, *Small* **2018**, *14*, 1703003.
- [47] K. Zhang, Y.-C. Lin, J. A. Robinson, *Semicond. Semimetals* **2016**, *95*, 189.
- [48] D. Kong, H. Wang, J. J. Cha, M. Pasta, K. J. Koski, J. Yao, Y. Cui, *Nano Lett.* **2013**, *13*, 1341.
- [49] S. Shin, Z. Jin, D. H. Kwon, R. Bose, Y.-S. Min, *Langmuir* **2015**, *31*, 1196.
- [50] H. Wang, D. Kong, P. Johannes, J. J. Cha, G. Zheng, K. Yan, N. Niu, Y. Cui, *Nano Lett.* **2013**, *13*, 3426.
- [51] H. Wang, Z. Lu, S. Xu, D. Kong, J. J. Cha, G. Zheng, P.-C. Hsu, K. Yan, D. Bradshaw, F. B. Prinz, Y. Cui, *Proc. Natl. Acad. Sci. USA* **2013**, *110*, 19701.
- [52] J. Kibsgaard, Z. Chen, B. N. Reinecke, T. F. Jaramillo, *Nat. Mater.* **2012**, *11*, 963.
- [53] L. Zhang, H. Wu, Y. Yan, X. Wang, X. Lou, *Energy Environ. Sci.* **2014**, *7*, 3302.
- [54] Y. Tan, P. Liu, L. Chen, W. Cong, Y. Ito, J. Han, X. Guo, Z. Tang, T. Fujita, A. Hirata, M. W. Chen, *Adv. Mater.* **2014**, *26*, 8023.
- [55] J. Ding, Y. Zhou, Y. Li, S. Guo, X. Huang, *Chem. Mater.* **2016**, *28*, 2074.
- [56] S. H. Choi, Y. N. Ko, J. Lee, Y. C. Kang, *Adv. Funct. Mater.* **2015**, *25*, 1780.
- [57] L. Zhang, T. Wang, L. Sun, Y. Sun, T. Hu, K. Xu, F. Ma, *J. Mater. Chem. A* **2017**, *5*, 19752.
- [58] Y. Liu, L. Ren, Z. Zhang, X. Qi, H. Li, J. Zhong, *Sci. Rep.* **2016**, *6*, 22516.
- [59] M. Zou, J. Zhang, H. Zhu, M. Du, Q. Wang, M. Zhang, X. Zhang, *J. Mater. Chem. A* **2015**, *3*, 12149.
- [60] D. Voiry, H. Yamaguchi, J. Li, R. Silva, D. C. B. Alves, T. Fujita, M. Chen, T. Asefa, V. B. Shenoy, G. Eda, M. Chhowalla, *Nat. Mater.* **2013**, *12*, 850.
- [61] Y. Zhang, J. Shi, G. Han, M. Li, Q. Ji, D. Ma, Y. Zhang, C. Li, X. Lang, Y. Zhang, Z. Liu, *Nano Res.* **2015**, *8*, 2881.
- [62] J. Shi, D. Ma, G.-F. Han, Y. Zhang, Q. Ji, T. Gao, J. Sun, X. Song, C. Li, Y. Zhang, X.-Y. Lang, Y. Zhang, Z. Liu, *ACS Nano* **2014**, *8*, 10196.
- [63] D. Voiry, M. Salehi, R. Silva, T. Fujita, M. Chen, T. Asefa, V. B. Shenoy, G. Eda, M. Chhowalla, *Nano Lett.* **2013**, *13*, 6222.
- [64] Y. Li, L. Wang, S. Zhang, X. Dong, Y. Song, T. Cai, Y. Liu, *Catal. Sci. Technol.* **2017**, *7*, 718.
- [65] J. Xie, H. Zhang, S. Li, R. Wang, X. Sun, M. Zhou, J. Zhou, X. W. D. Lou, Y. Xie, *Adv. Mater.* **2013**, *25*, 5807.
- [66] Y. Li, K. Yin, L. Wang, X. Lu, Y. Zhang, Y. Liu, D. Yan, Y. Song, S. Luo, *Appl. Catal., B* **2018**, *239*, 537.
- [67] K. Chang, X. Hai, H. Pang, H. Zhang, L. Shi, G. Liu, H. Liu, G. Zhao, M. Li, J. Ye, *Adv. Mater.* **2016**, *28*, 10033.
- [68] Q. He, L. Wang, K. Yin, S. Luo, *Nanoscale Res. Lett.* **2018**, *13*, 167.
- [69] C. Tan, Z. Luo, A. Chaturvedi, Y. Cai, Y. Du, Y. Gong, Y. Huang, Z. Lai, X. Zhang, L. Zheng, X. Qi, M. H. Goh, J. Wang, S. Han, X.-J. Wu, L. Gu, C. Kloc, H. Zhang, *Adv. Mater.* **2018**, *30*, 1705509.
- [70] L. Lin, *Ph.D. Thesis*, University of Sheffield **2013**.
- [71] L. Lin, N. Miao, J. Huang, S. Zhang, Y. Zhu, D. D. Horsell, P. Ghosez, Z. Sun, D. A. Allwood, *Nano Energy* **2017**, *38*, 544.
- [72] G. Ye, Y. Gong, J. Lin, B. Li, Y. He, S. T. Pantelides, W. Zhou, R. Vajtai, P. M. Ajayan, *Nano Lett.* **2016**, *16*, 1097.
- [73] H. Li, Y. Tan, P. Liu, C. Guo, M. Luo, J. Han, T. Lin, F. Huang, M. Chen, *Adv. Mater.* **2016**, *28*, 8945.
- [74] J. N. Coleman, M. Lotya, A. O'Neill, S. D. Bergin, P. J. King, U. Khan, K. Young, A. Gaucher, S. De, R. J. Smith, I. V. Shvets, S. K. Arora, G. Stanton, H.-Y. Kim, K. Lee, G. T. Kim, G. S. Duesberg, T. Hallam, J. J. Boland, J. J. Wang, J. F. Donegan, J. C. Grunlan, G. Moriarty, A. Shmeliov, R. J. Nicholls, J. M. Perkins, E. M. Grieveson, K. Theuvsen, D. W. McComb, P. D. Nellist, V. Nicolosi, *Science* **2011**, *331*, 568.
- [75] Z. Lei, S. Xu, P. Wu, *Phys. Chem. Chem. Phys.* **2016**, *18*, 70.
- [76] L. Lin, Y. Xu, S. Zhang, I. M. Ross, A. C. M. Ong, D. A. Allwood, *ACS Nano* **2013**, *7*, 8214.
- [77] S. Xu, D. Li, P. Wu, *Adv. Funct. Mater.* **2015**, *25*, 1127.
- [78] H. Li, R. Y. Tay, S. H. Tsang, X. Zhen, E. H. T. Teo, *Small* **2015**, *11*, 6491.
- [79] S. Jeong, D. Yoo, M. Ahn, P. Miró, T. Heine, J. Cheon, *Nat. Commun.* **2015**, *6*, 5763.
- [80] Y. Ouyang, C. Ling, Q. Chen, Z. Wang, L. Shi, J. Wang, *Chem. Mater.* **2016**, *28*, 4390.
- [81] J. Hong, Z. Hu, M. Probert, K. Li, D. Lv, X. Yang, L. Gu, N. Mao, Q. Feng, L. Xie, J. Zhang, D. Wu, Z. Zhang, C. Jin, W. Ji, X. Zhang, J. Yuan, Z. Zhang, *Nat. Commun.* **2015**, *6*, 6293.
- [82] S. Najmaei, Z. Liu, W. Zhou, X. Zou, G. Shi, S. Lei, B. I. Yakobson, J.-C. Idrobo, P. M. Ajayan, J. Lou, *Nat. Mater.* **2013**, *12*, 754.
- [83] Q. Ma, P. M. Odenthal, J. Mann, D. Le, C. S. Wang, Y. Zhu, T. Chen, D. Sun, K. Yamaguchi, T. Tran, M. Wurch, J. L. McKinley, J. Wyrick, K. Magnone, T. F. Heinz, T. S. Rahman, R. Kawakami, L. Bartels, *J. Phys.: Condens. Matter* **2013**, *25*, 252201.
- [84] H.-P. Komsa, J. Kotakoski, S. Kurasch, O. Lehtinen, U. Kaiser, A. V. Krasheninnikov, *Phys. Rev. Lett.* **2012**, *109*, 035503.
- [85] D. Liu, Y. Guo, L. Fang, J. Robertson, *Appl. Phys. Lett.* **2013**, *103*, 183113.
- [86] H. Li, C. Tsai, A. L. Koh, L. Cai, A. W. Contryman, A. H. Fragapane, J. Zhao, H. S. Han, H. C. Manoharan, F. Abild-Pedersen, J. K. Nørskov, X. Zheng, *Nat. Mater.* **2016**, *15*, 48.
- [87] B. Yildiz, *MRS Bull.* **2014**, *39*, 147.
- [88] W. Zhou, X. Zou, S. Najmaei, Z. Liu, Y. Shi, J. Kong, J. Lou, P. M. Ajayan, B. I. Yakobson, J.-C. Idrobo, *Nano Lett.* **2013**, *13*, 2615.
- [89] A. W. Bott, *Curr. Sep.* **1998**, *17*, 87.
- [90] A. Liu, L. Zhao, J. Zhang, L. Lin, H. Wu, *ACS Appl. Mater. Interfaces* **2016**, *8*, 25210.
- [91] M. A. Lukowski, A. S. Daniel, F. Meng, A. Forticaux, L. Li, S. Jin, *J. Am. Chem. Soc.* **2013**, *135*, 10274.
- [92] D. Merki, H. Vruble, L. Rovelli, S. Fierro, X. Hu, *Chem. Sci.* **2012**, *3*, 2515.
- [93] J. Deng, H. Li, J. Xiao, Y. Tu, D. Deng, H. Yang, H. Tian, J. Li, P. Ren, X. Bao, *Energy Environ. Sci.* **2015**, *8*, 1594.
- [94] X. Dai, K. Du, Z. Li, M. Liu, Y. Ma, H. Sun, X. Zhang, Y. Yang, *ACS Appl. Mater. Interfaces* **2015**, *7*, 27242.
- [95] X. Zhang, F. Meng, S. Mao, Q. Ding, M. J. Shearer, M. S. Faber, J. Chen, R. J. Hamers, S. Jin, *Energy Environ. Sci.* **2015**, *8*, 862.
- [96] X.-J. Lv, G.-W. She, S.-X. Zhou, Y.-M. Li, *RSC Adv.* **2013**, *3*, 21231.
- [97] X. Ren, Q. Ma, H. Fan, L. Pang, Y. Zhang, Y. Yao, X. Ren, S. (F) Liu, *Chem. Commun.* **2015**, *51*, 15997.
- [98] C. Sun, J. Zhang, J. Ma, P. Liu, D. Gao, K. Tao, D. Xue, *J. Mater. Chem. A* **2016**, *4*, 11234.

- [99] T. A. Shifa, F. Wang, K. Liu, Z. Cheng, K. Xu, Z. Wang, X. Zhan, C. Jiang, J. He, *Small* **2017**, *13*, 1603706.
- [100] A. Jiang, B. Zhang, Z. Li, G. Jin, J. Hao, *Chem. - Asian J.* **2018**, *13*, 1438.
- [101] X. Ren, Q. Ma, P. Ren, Y. Wang, *Int. J. Hydrogen Energy* **2018**, *43*, 15275.
- [102] Y. Zhao, W. Wang, C. Li, L. He, *Sci. Rep.* **2017**, *7*, 17088.
- [103] G. Zhang, X. Zheng, Q. Xu, J. Zhang, W. Liu, J. Chen, *J. Mater. Chem. A* **2018**, *6*, 4793.
- [104] Y. Qu, H. Pan, C. T. Kwok, Z. Wang, *Nanoscale Res. Lett.* **2015**, *10*, 480.
- [105] J. Xie, J. Zhang, S. Li, F. Grote, X. Zhang, H. Zhang, R. Wang, Y. Lei, B. Pan, Y. Xie, *J. Am. Chem. Soc.* **2013**, *135*, 17881.
- [106] D. Voiry, A. Goswami, R. Koppera, C. de C. C. e Silva, D. Kaplan, T. Fujita, M. Chen, T. Asefa, M. Chhowalla, *Nat. Chem.* **2015**, *7*, 45.
- [107] Q. Tang, D. Jiang, *Chem. Mater.* **2015**, *27*, 3743.
- [108] X. Shi, M. Fields, J. Park, J. M. McEnaney, H. Yan, Y. Zhang, C. Tsai, T. F. Jaramillo, R. Sinclair, J. K. Nørskov, X. Zheng, *Energy Environ. Sci.* **2018**, *11*, 2270.
- [109] H. Wang, C. Tsai, D. Kong, K. Chan, F. Abild-Pedersen, J. K. Nørskov, Y. Cui, *Nano Res.* **2015**, *8*, 566.
- [110] P. Liu, J. Zhu, J. Zhang, P. Xi, K. Tao, D. Gao, D. Xue, *ACS Energy Lett.* **2017**, *2*, 745.
- [111] D. Gao, B. Xia, C. Zhu, Y. Du, P. Xi, D. Xue, J. Ding, J. Wang, *J. Mater. Chem. A* **2018**, *6*, 510.
- [112] T. Kou, T. Smart, B. Yao, I. Chen, D. Thota, Y. Ping, Y. Li, *Adv. Energy Mater.* **2018**, *8*, 1703538.
- [113] T. H. M. Lau, X. Lu, J. Kulhavý, S. Wu, L. Lu, T.-S. Wu, R. Kato, J. S. Foord, Y.-L. Soo, K. Suenaga, S. C. E. Tsang, *Chem. Sci.* **2018**, *9*, 4769.
- [114] X. Chen, Y. Qiu, G. Liu, W. Zheng, W. Feng, F. Gao, W. Cao, Y. Fu, W. Hu, P. Hu, *J. Mater. Chem. A* **2017**, *5*, 11357.
- [115] R. Li, L. Yang, T. Xiong, Y. Wu, L. Cao, D. Yuan, W. Zhou, *J. Power Sources* **2017**, *356*, 133.
- [116] L. Bian, W. Gao, J. Sun, M. Han, F. Li, Z. Gao, L. Shu, N. Han, Z. Yang, A. Song, Y. Qu, J. C. Ho, *ChemCatChem* **2018**, *10*, 1571.
- [117] K. Guruprasad, T. Maiyalagan, S. Shanmugam, *ACS Appl. Energy Mater.* **2019**, *2*, 6184.
- [118] Q. Yang, Z. Wang, L. Dong, W. Zhao, Y. Jin, L. Fang, B. Hu, M. Dong, *J. Phys. Chem. C* **2019**, *123*, 10917.
- [119] F. Zhang, Y. Lu, D. S. Schulman, T. Zhang, K. Fujisawa, Z. Lin, Y. Lei, A. L. Elias, S. Das, S. B. Sinnott, M. Terrones, *Sci. Adv.* **2019**, *5*, eaav5003.
- [120] J. Zhang, S. Jia, I. Kholmanov, L. Dong, D. Er, W. Chen, H. Guo, Z. Jin, V. B. Shenoy, L. Shi, J. Lou, *ACS Nano* **2017**, *11*, 8192.
- [121] Y. Zhou, E. Song, J. Zhou, J. Lin, R. Ma, Y. Wang, W. Qiu, R. Shen, K. Suenaga, Q. Liu, J. Wang, Z. Liu, J. Liu, *ACS Nano* **2018**, *12*, 4486.
- [122] A.-Y. Lu, H. Zhu, J. Xiao, C.-P. Chuu, Y. Han, M.-H. Chiu, C.-C. Cheng, C.-W. Yang, K.-H. Wei, Y. Yang, Y. Wang, D. Sokaras, D. Nordlund, P. Yang, D. A. Muller, M.-Y. Chou, X. Zhang, L.-J. Li, *Nat. Nanotechnol.* **2017**, *12*, 744.
- [123] D. Er, H. Ye, N. C. Frey, H. Kumar, J. Lou, V. B. Shenoy, *Nano Lett.* **2018**, *18*, 3943.
- [124] Q. Xiong, J. Zhou, J. Zhang, T. Kitamura, Z. Li, *Phys. Chem. Chem. Phys.* **2018**, *20*, 20988.
- [125] Y. Guo, S. Zhou, Y. Bai, J. Zhao, *Appl. Phys. Lett.* **2017**, *110*, 163102.
- [126] W. Shi, Z. Wang, *J. Phys.: Condens. Matter* **2018**, *30*, 215301.
- [127] Z. Zhao, F. Qin, S. Kasiraju, L. Xie, M. K. Alam, S. Chen, D. Wang, Z. Ren, Z. Wang, L. C. Grabow, J. Bao, *ACS Catal.* **2017**, *7*, 7312.
- [128] M. Shao, Y. Shao, S. Ding, R. Tong, X. Zhong, L. Yao, W. F. Ip, B. Xu, X.-Q. Shi, Y.-Y. Sun, X. Wang, H. Pan, *ACS Sustainable Chem. Eng.* **2019**, *7*, 4220.
- [129] J. Jeon, Y. Park, S. Choi, J. Lee, S. S. Lim, B. H. Lee, Y. J. Song, J. H. Cho, Y. H. Jang, S. Lee, *ACS Nano* **2018**, *12*, 338.
- [130] J. R. Kitchin, J. K. Nørskov, M. A. Barteau, J. G. Chen, *Catal. Today* **2005**, *105*, 66.
- [131] D. J. Ham, J. S. Lee, *Energies* **2009**, *2*, 873.
- [132] C. Liu, Y. Wen, L. Lin, H. Zhang, X. Li, S. Zhang, *Int. J. Hydrogen Energy* **2018**, *43*, 15650.
- [133] K. Zhang, Y. Zhao, S. Zhang, H. Yu, Y. Chen, P. Gao, C. Zhu, *J. Mater. Chem. A* **2014**, *2*, 18715.
- [134] Y. Li, X. Wu, H. Zhang, J. Zhang, *ACS Appl. Energy Mater.* **2018**, *1*, 3377.
- [135] C. Tang, W. Wang, A. Sun, C. Qi, D. Zhang, Z. Wu, D. Wang, *ACS Catal.* **2015**, *5*, 6956.
- [136] H. Ang, H. T. Tan, Z. M. Luo, Y. Zhang, Y. Y. Guo, G. Guo, H. Zhang, Q. Yan, *Small* **2015**, *11*, 6278.
- [137] Y. Huang, H. Lu, H. Gu, J. Fu, S. Mo, C. Wei, Y.-E. Miao, T. Liu, *Nanoscale* **2015**, *7*, 18595.
- [138] H. Tang, K. Dou, C.-C. Kaun, Q. Kuang, S. Yang, *J. Mater. Chem. A* **2014**, *2*, 360.
- [139] S. Kamila, B. Mohanty, A. K. Samantara, P. Guha, A. Ghosh, B. Jena, P. V. Satyam, B. K. Mishra, B. Kumar, *Sci. Rep.* **2017**, *7*, 8378.
- [140] K. Ojha, S. Saha, S. Banerjee, A. K. Ganguli, *ACS Appl. Mater. Interfaces* **2017**, *9*, 19455.
- [141] S. Yang, Y. Zhang, S. Wang, J. Shi, X. Liu, L. Li, *J. Mater. Chem. A* **2019**, *7*, 23886.
- [142] G. Solomon, R. Mazaaro, S. You, M. M. Natile, V. Morandi, I. Concina, A. Vomiero, *ACS Appl. Mater. Interfaces* **2019**, *11*, 22380.
- [143] L. Yang, W. Zhou, D. Hou, K. Zhou, G. Li, Z. Tang, L. Li, S. Chen, *J. Mater. Chem. A* **2015**, *7*, 5203.
- [144] M. Sarno, A. Garamella, C. Cirillo, P. Ciambelli, *Chem. Eng. Trans.* **2014**, *41*, 385.
- [145] S.-K. Park, D. Y. Chung, D. Ko, Y.-E. Sung, Y. Piao, *J. Mater. Chem. A* **2016**, *4*, 12720.
- [146] R. Subbaraman, D. Tripkovic, D. Strmcnik, K.-C. Chang, M. Uchimura, A. P. Paulikas, V. Stamenkovic, N. M. Markovic, *Science* **2011**, *334*, 1256.
- [147] L. Ledezma-Yanez, W. D. Z. Wallace, P. Sebastián-Pascual, V. Climent, J. M. Feliu, M. T. M. Koper, *Nat. Energy* **2017**, *2*, 17031.
- [148] J. Liu, Y. Zheng, D. Zhu, A. Vasileff, T. Ling, S.-Z. Qiao, *Nanoscale* **2017**, *9*, 16616.
- [149] J. Hu, C. Zhang, L. Jiang, H. Lin, Y. An, D. Zhou, M. K. H. Leung, S. Yang, *Joule* **2017**, *1*, 383.
- [150] Z. Wu, M. Song, X. Liu, *J. Electrochem. Soc.* **2018**, *165*, F976.
- [151] Y. Huang, Y. Sun, X. Zheng, T. Aoki, B. Pattengale, J. Huang, X. He, W. Bian, S. Younan, N. Williams, J. Hu, J. Ge, N. Pu, X. Yan, X. Pan, L. Zhang, Y. Wei, J. Gu, *Nat. Commun.* **2019**, *10*, 982.
- [152] Y. Zhang, S. Niu, Y. Wu, X. Zheng, J. Cai, J. Ye, Y. Xie, Y. Liu, J. Zhou, J. Zhu, X. Liu, G. Wang, Y. Qian, *Nat. Commun.* **2019**, *10*, 1217.
- [153] X. Zhang, Y. Liang, *Adv. Sci.* **2018**, *5*, 1700644.
- [154] D. Voiry, R. Fullon, J. Yang, C. de Carvalho Castro e Silva, R. Koppera, I. Bozkurt, D. Kaplan, M. J. Lagos, P. E. Batson, G. Gupta, A. D. Mohite, L. Dong, D. Er, V. B. Shenoy, T. Asefa, M. Chhowalla, *Nat. Mater.* **2016**, *15*, 1003.
- [155] R. Koppera, D. Voiry, S. E. Yalcin, B. Branch, G. Gupta, A. D. Mohite, M. Chhowalla, *Nat. Mater.* **2014**, *13*, 1128.
- [156] R. Koppera, D. Voiry, S. E. Yalcin, W. Jen, M. Acerce, S. Torrel, B. Branch, S. Lei, W. Chen, S. Najmaei, J. Lou, P. M. Ajayan, G. Gupta, A. D. Mohite, M. Chhowalla, *APL Mater.* **2014**, *2*, 092516.
- [157] D. Vikraman, S. Hussain, K. Akbar, L. Truong, A. Kathalingam, S.-H. Chun, J. Jung, H. J. Park, H.-S. Kim, *ACS Sustainable Chem. Eng.* **2018**, *6*, 8400.
- [158] K. C. Kwon, S. Choi, K. Hong, C. W. Moon, Y.-S. Shim, D. H. Kim, T. Kim, W. Sohn, J.-M. Jeon, C.-H. Lee, K. T. Nam, S. Han, S. Y. Kim, H. W. Jang, *Energy Environ. Sci.* **2016**, *9*, 2240.

- [159] J. Greeley, T. F. Jaramillo, J. Bonde, I. Chorkendorff, J. K. Nørskov, *Nat. Mater.* **2006**, *5*, 909.
- [160] M. Fang, W. Gao, G. Dong, Z. Xia, S. Yip, Y. Qin, Y. Qu, J. C. Ho, *Nano Energy* **2016**, *27*, 247.
- [161] J. F. Gallejas, C. G. Read, C. W. Roske, N. S. Lewis, R. Schaak, *Chem. Mater.* **2016**, *28*, 6017.
- [162] S. Saha, K. V. Ramanujachary, S. E. Lofland, A. K. Ganguli, *Mater. Res. Express* **2016**, *3*, 016501.
- [163] S. Ye, F. Luo, Q. Zhang, P. Zhang, T. Xu, Q. Wang, D. He, L. Guo, Y. Zhang, C. He, X. Ouyuan, M. Gu, J. Liu, X. Sun, *Energy Environ. Sci.* **2019**, *12*, 1000.
- [164] M. Li, Q. Ma, W. Zhi, X. Liu, X. Zhu, S. Liu, *Sci. Adv.* **2015**, *1*, e1400268.
- [165] J. Zhang, Y. Zhao, X. Guo, C. Chen, C.-L. Dong, R.-S. Liu, C.-P. Han, Y. Li, Y. Gogotsi, G. Wang, *Nat. Catal.* **2018**, *1*, 985.
- [166] A. Kumatani, C. Miura, H. Kuramochi, T. Ohto, M. Wakisaka, Y. Nagata, H. Ida, Y. Takahashi, K. Hu, S. Jeong, J.-i. Fujita, T. Matsue, *Adv. Sci.* **2019**, *6*, 1900119.
- [167] B. R. Sathe, X. X. Zou, T. Asefa, *Catal. Sci. Technol.* **2014**, *4*, 2023.
- [168] L. Yang, X. Wang, J. Wang, G. Cui, D. Liu, *Nanotechnology* **2018**, *29*, 345705.
- [169] B. Zhang, H.-H. Wang, H. Su, L.-B. Lv, T.-J. Zhao, J.-M. Ge, X. Wei, K.-X. Wang, X.-H. Li, J.-S. Chen, *Nano Res.* **2016**, *9*, 2606.
- [170] Y. Zheng, Y. Jiao, L. H. Li, T. Xing, Y. Chen, M. Jaroniec, S. Z. Qiao, *ACS Nano* **2014**, *8*, 5290.
- [171] L. Lin, W. Lei, S. Zhang, Y. Liu, G. G. Wallace, J. Chen, *Energy Storage Mater.* **2019**, *19*, 408.
- [172] J. Kibsgaard, C. Tsai, K. Chan, J. D. Benck, J. K. Nørskov, F. Abild-Pedersen, T. F. Jaramillo, *Energy Environ. Sci.* **2015**, *8*, 3022.
- [173] A. B. Laursen, K. R. Patraju, M. K. Whitaker, M. Retuerto, T. Sarkar, N. Yao, K. V. Ramanujachary, M. Greenblatt, G. C. Dismukes, *Energy Environ. Sci.* **2015**, *8*, 1027.
- [174] J. Tian, Q. Liu, Y. Liang, Z. Xing, A. M. Asiri, X. Sun, *ACS Appl. Mater. Interfaces* **2014**, *6*, 20579.
- [175] J. F. Callejas, C. G. Read, C. W. Roske, N. S. Lewis, R. E. Schaak, *Chem. Mater.* **2016**, *28*, 6017.
- [176] K. K. Dey, S. Jha, A. Kumar, G. Gupta, A. K. Srivastava, P. P. Ingole, *Electrochim. Acta* **2019**, *312*, 89.
- [177] M. S. Burke, L. J. Enman, A. S. Batchellor, S. Zou, S. W. Bottcher, *Chem. Mater.* **2015**, *27*, 7549.
- [178] M. P. Browne, Z. Sofer, M. Pumera, *Energy Environ. Sci.* **2019**, *12*, 41.
- [179] Z. Lu, H. Wang, D. Kong, K. Yan, P.-C. Hsu, G. Zheng, H. Yao, Z. Liang, X. Sun, Y. Cui, *Nat. Commun.* **2014**, *5*, 4345.
- [180] Z. W. Seh, K. D. Fredrickson, B. Anasori, J. Kibsgaard, A. L. Strickler, M. R. Lukatskaya, Y. Gogotsi, T. F. Jaramillo, A. Vojvodic, *ACS Energy Lett.* **2016**, *1*, 589.
- [181] J. Peng, X. Chen, W.-J. Ong, X. Zhao, N. Li, *Chem* **2019**, *5*, 18.
- [182] E. G. da Silveria Firmiano, A. C. Rabelo, C. J. Dalmaschio, A. N. Pinheiro, E. C. Pereria, W. H. Schreiner, E. R. Leite, *Adv. Energy Mater.* **2014**, *4*, 1301380.
- [183] L. Zhao, C. Hong, L. Lin, H. Wu, Y. Su, X. Zhang, A. Liu, *Carbon* **2017**, *116*, 223.
- [184] X. Zheng, X. Xiong, J. Yang, D. Chen, R. Jian, L. Lin, *Chem. Eng. J.* **2018**, *333*, 153.
- [185] X. Zheng, H. Cheng, J. Yang, D. Chen, R. Jian, L. Lin, *ACS Appl. Nano Mater.* **2018**, *1*, 2754.
- [186] D. Mombrú, R. Faccio, Á. W. Mombrú, *Appl. Surf. Sci.* **2018**, *462*, 409.
- [187] D. Chen, X. Zhang, J. Tang, H. Cui, Y. Li, *Appl. Phys. A* **2018**, *124*, 194.
- [188] J. Zhang, J. Wu, H. Gao, W. Chen, J. Yuan, U. Martinez, G. Gupta, A. Mohite, P. M. Ajayan, J. Lou, *Adv. Mater.* **2017**, *29*, 1701955.
- [189] E. Mitterreiter, Y. Liang, M. Golibrzuch, D. McLaughlin, C. Csoklich, J. D. Bartl, A. Holleitner, U. Wurstbauer, A. S. Bandarenka, *npj 2D Mater. Appl.* **2019**, *3*, 25.
- [190] B. C. Bayer, R. Kainhard, M. Reza, A. Monazam, T. Susi, J. Kotakoski, T. Gupta, D. Eder, W. Waldhauser, J. C. Meyer, *ACS Nano* **2018**, *12*, 8758.
- [191] B. T. Hartman, C. S. Wondergem, N. Kumar, A. van den Berg, B. M. Weckhusen, *J. Phys. Chem. Lett.* **2016**, *7*, 1570.
- [192] X. Chen, A. R. McDonald, *Adv. Mater.* **2016**, *28*, 5738.
- [193] D. Sarkar, X. Xie, J. Kang, H. Zhang, W. Liu, J. Navarrete, M. Moskovits, K. Banerjee, *Nano Lett.* **2015**, *15*, 2852.
- [194] D.-H. Kang, S. R. Pae, J. Shim, G. Yoo, J. Jeon, J. W. Leem, J. S. Yu, S. Lee, B. Shin, J.-H. Park, *Adv. Mater.* **2016**, *28*, 7799.
- [195] X. Huang, B. Zheng, Z. Liu, C. Tan, J. Liu, B. Chen, H. Li, J. Chen, X. Zhang, Z. Fan, W. Zhang, Z. Guo, F. Huo, Y. Yang, L.-H. Xie, W. Huang, H. Zhang, *ACS Nano* **2014**, *8*, 8695.
- [196] M. I. Gonzalez, A. B. Turkiewicz, L. E. Darago, J. Oktawiec, K. Bustillo, F. Grandjean, G. J. Long, J. R. Long, *Nature* **2020**, *577*, 64.
- [197] X. Zhang, Z. Zhang, D. Wu, X. Zhang, X. Zhao, Z. Zhou, *Small Methods* **2018**, *2*, 1700359.
- [198] S. Seo, S. Kim, H. Choi, J. Lee, H. Yoon, G. Piao, J. Park, Y. Jung, J. Song, S. Y. Jeong, H. Park, S. Lee, *Adv. Sci.* **2019**, *6*, 1900301.
- [199] F. M. Pesci, M. S. Sokolikova, C. Grotta, P. C. Sherrell, F. Reale, K. Sharda, N. Ni, P. Palczynski, C. Mattevi, *ACS Catal.* **2017**, *7*, 4990.
- [200] P. C. Sherrell, P. Palczynski, M. S. Sokolikova, F. Reale, F. M. Pesci, M. Och, C. Mattevi, *ACS Appl. Energy Mater.* **2019**, *2*, 5877.
- [201] S. Zhu, P. Pochet, H. T. Johnson, *ACS Nano* **2019**, *13*, 6925.
- [202] G. Iannaccone, F. Bonaccorso, L. Colombo, G. Fiori, *Nat. Nanotechnol.* **2018**, *13*, 183.
- [203] T. K. Patra, F. Zhang, D. S. Schulman, H. Chan, M. J. Cherukara, M. Terrones, S. Das, B. Narayanan, S. K. R. S. Sankaranarayanan, *ACS Nano* **2018**, *12*, 8006.
- [204] S. H. Noh, J. Hwang, J. Kang, M. H. Seo, D. Choi, B. Han, *J. Mater. Chem. A* **2018**, *6*, 20005.